Comparison of Out-of-Field Organ Doses from IMRT Plans for Head and Neck Involving the Varian Clinac (TRILOGY) and TomoTherapy Hi-Art II System

by

Amatare Alphonsus Dorgu

A Thesis Submitted to the Graduate

Faculty of Rensselaer Polytechnic Institute

in Partial Fulfillment of the

Requirements for the degree of

MASTER OF SCIENCE

Major Subject: NUCLEAR ENGINEERING

Approved:

_____

Xie George Xu, Thesis Adviser

Rensselaer Polytechnic Institute
Troy, New York

April, 2009
(For Graduation May 2009)

CONTENTS

LIST OF TABLES

LIST OF FIGURES

ACKNOWLEDGMENT

I would like to first acknowledge God for giving me a chance at life and bestowing in me the desire to want to improve the quality of life of people. I also want to thank God for blessing me with my wife, Oiza and our children, Tarenemi and Amatare, whom have been a constant source of inspiration and joy; especially Oiza for encouraging me to follow my dreams at RPI and providing the support, only a loving wife could, throughout my studies at RPI. Also, my mother in-law Frances Uyanwune, for her invaluable words of encouragement and for taking the risk of many long trips from Connecticut to provide assistance with the kids, enabling me spend more time on my studies.

Also, I want to show deep appreciation and thanks to my thesis advisor, Dr George Xu, for his great guidance and direction during my studies at RPI. You listened to my concerns and gave excellent advice that was a source of motivation for me. Finally to Dan Pavord, the chief medical physicist and all the staff of Vassar Brothers Medical Center's Dyson Center for Cancer care, for their kindness and support in making the medical physics division a conducive place to study and learn.

ABSTRACT

As a result of leakage and scatter radiation, patients undergoing external-beam radiation treatment receive out-of-Field organ doses from three dimensional conformal radiation therapy (3DCRT) to intensity modulated radiation therapy (IMRT). Currently there are no established computational tools that can effectively estimate and predict such dose and risk. This research work is focused on the measurement and comparison of absorbed dose to organs due to scatter radiation from the phantom and leakage radiation from the treatment machine. The measurements record secondary-scatter-radiation-dose as a result of IMRT of a complex tumor distribution in the head and neck region specific to a nasopharyngeal cancer (NPC) case. A physical male anthropomorphic phantom (ATOM®) is used for the measurements in two configurations: 1) with all the transverse cross sectional slices of the Adult Male ATOM® phantom intact. 2) Without the transverse cross sectional slices in the region representing the Planning Treatment Volume (PTV).

The IMRT plans are delivered to the phantom, using two widely used radiation therapy delivery systems – the Varian Clinac (TRILOGY) and TomoTherapy® Hi.Art® II system (TOMO). A comparison of dose deposited to organs out of the treatment field, was made under similar conditions - same energy 6MV, and similar treatment plans. The organs outside the treatment field that was studied include the brain, lungs, esophagus, liver, kidneys, stomach, prostate, bladder and testis. The analysis and results in this work show a similar trend in the total out-of-field organ dose. However a marked difference in the specific behavior of the ratio of scatter-components of out-of-field organ dose to the total dose is found for TRILOGY showing a slow and not-so-steep decline in which the scatter component contributes the smaller portion of the total Out-of-field dose, ranging between 25-0% from the brain to the testis and leakage radiation component contributes the larger portion of the total dose, ranging between 75-100% of the total dose ; in contrast to 75 – 0% and 25 – 100% respectively for TOMO . It is clear from this study that more in depth investigation is needed in the future on new and emerging modalities in order to establish a large database of actual measurement of various radiation therapy modalities and to develop a necessary insight into ways to reduce the second cancer induction in cancer survivors who are treated by radiation.

1. Introduction

In the current paradigm of treatment planning involving external beams, the focus is on effective irradiation of the Gross Tumor Volume (GTV) and delivery of prescription dose to cancerous cells within the Clinical Target Volume (CTV) which encompassing the GTV, while simultaneously limiting the irradiation of critical structures called Organs-At-Risk (OAR) within close proximity of the tumor volume. The tumor and clinical Planning Target Volumes (PTV) which consists of the CTV and a margin to account for change in size, shape, and position relative to the treatment beams(s) are defined from volume specified in International Commission on Radiation Units and Measurements (ICRU) Report 50 (ICRU 2003).

Existing treatment planning algorithms are based on old modalities and do not take into account of biological effects that can occur in health tissues. As radiation therapy moved towards intensity modulation, improvement in local tumor control and in treating more complex cancer cases has been realized. These advances are beginning to help yield a greater surviving rate among cancer patients. However, new modalities are based on more complicated delivery systems, thus requiring longer times to delivery a prescribed radiation dose to the target. A direct consequence of the longer treatment times and sophistication in external beam therapy is the increased exposure of healthy organs in patients to ionizing radiation. This exposure can come in the form of leakage radiation from the linear- accelerator (Linac) treatment head, leakage radiation from the body of the linac and secondary radiation from the body of the patient due to scatter of the primary beam (Bednarz 2008). It has also been highlighted that this increased exposure due to emerging treatment modalities, which include intensity-modulated radiation treatment (IMRT), carries with it the associated increase in probability of elevated doses to organs that are out of the treatment field (Xu et al. 2008).

This research work is focused on the measurement of absorbed dose to organs out of the treatment field as well as the determination of out-of-field dose contributions due to scatter radiation from the phantom and leakage radiation from the treatment machine. The measurements record secondary-scatter-radiation-dose as a result of IMRT of a complex tumor distribution in the head and neck region specific to a nasopharyngeal cancer (NPC) case.

1.1 Intensity Modulated Radiation Therapy (IMRT)

IMRT has be described as a radiation therapy technique in which nonuniform fluence is delivered to the patient from any given position of the treatment beam to optimize the composite dose distribution (Khan 2003). It has also been explained that this modulation can be achieved spatially by continuously interrupting an otherwise uniform flow of X-rays via collimation and or compensation; as well as by creating a spatial variation by temporally modulating the fluence and varying the temporal modulation in space (Webb 2003a). Consequently, this ability to modulate the X-ray beam-elements (bixels) in a three dimensional field that has been shaped to conform to the tumor target volume, gives IMRT its added flexibility in dose escalation to tumor and dose avoidance to the organs-at-risk.

1.1.1 Historical Review of IMRT

IMRT is based on the principles of X- ray discovered in 1895 in Germany by Roentgen (Röntgen 1895). IMRT was well established in several geographically distributed centers by 2003 (Webb 2003b). It has also been suggested that IMRT was 'invented' based on work by Brahme et al. in 1982 (Bortfeld 2006), in which they discussed inverse-planning for a fairly special case of rotational symmetry Webb 2003b). This invention marks the point at which the modern IMRT idea emerges in which use of inverse planning amongst other planning methods are used to optimize the shape of a dose distribution, with the capability of generating concave dose distributions and providing specific spearing of sensitive normal structures within complex treatment geometries (IMRT-CWG 2001). However in pointing out the history of IMRT, it is important to note the main technological precursors as the development of image-based three dimensional radiation treatment planning (3D-RTP) systems and the development of computer-controlled delivery systems as pointed out in the literature (IMRT-CWG 2001).

Also, based on the literature, the late 1800s was the period in which doctors realized the importance of focusing radiation to a cancerous target but had no established

methods of achieving this goal. It would follow that the late 1950s was the period in which Takahashi first discussed conformation therapy and the first multileaf collimator (MLC) was invented. This lead to the work in 1965 by Takahashi and his colleagues who planned and delivered dynamic treatments in what was probably the first multileaf collimator system, in Nagoya Japan (IMRT-CWG 2001). The 1970s was the period in which the Royal Northern Hospital in England pioneered computer controlled conformal radiation therapy work by building the "tracking cobalt unit" which attempted to track and conform to the path of a diseased area; the Joint Center from the Harvard Medical School also contributed to this kind of work during this period. The 1980s then followed with the seminal paper by Brahme et al, mentioned above as well as other import contributions from Convery, Rosenbloom, Kallman, Webb, Bortfeld, Boyer, Mackie, Stein, Svensson, and Spirou during the 1980s and 1990s. All these contributions culminated in the introduction of commercial TomoTherapy in 2002 as well as a large number of competing IMRT planning systems in 2003 (Webb 2003b).

1.2 Out –of-Field Dosimetry

On one hand dosimetry is the determination by measurement or calculation of the absorbed dose or dose rate resulting from the interaction of ionizing radiation with matter; as well as any of the other radiologically relevant quantities such as Kerma, fluence, etc (Attix 2004); while on the other hand the term "out of field" has recently been described as a term frequently used in the literature to mean all locations inside a physical phantom outside of the field edge defined by the secondary collimators or the MLC in the accelerator (Bednarz 2008). Thus, out-of-field dosimetry is the determination of absorbed dose resulting from the interaction of ionizing radiation within locations inside a physical phantom or human being, outside of the treatment field defined by the MLC.

1.3 The Anthropomorphic Phantom for Measurements

In radiation dosimetry different types of physical and computational phantoms are used to make measurements, ranging in style from geometrical shapes (Squares, circles,

cylinders, and polygons) to human like anthropomorphic phantoms. In this work, a physical anthropomorphic adult male phantom named ATOM® Figure 1.1 is used to acquire out-of-field dosimetric data. The Atom phantom consists of 25mm thick, sectional slab slices, but differ from other dosimetry phantoms by providing optimized thermoluminescent- dosimeter (TLD) locations specific to 19 inner organs as suggested by the manufactures – CIRS Tissue Simulation Technology. It is also manufactured to produce tissue equivalent substitutes with tolerance better than 1% for bone and soft tissue and 3% for lung tissue at photon energies from 30 keV to 20 MeV.

Figure 1.1 The Physical Adult Male Anthropomorphic ATOM® phantom

1.4 Literature Review on Out-of-Field Dosimetry

1.4.1 Early Classical Treatment and Out-of-Field Dosimetry study

In a recent extensive review on out-of-field dosimetry, Xu et al. points out that "Fraass and van de Geijn (1983) were one of the first groups to perform detailed studies of the various components of out-of-field photon dose (Xu et al. 2008). The authors compared several megavoltage photon beams and characterized the dose outside the

treatment field as a function of beam energy. The group also devised a scheme to measure leakage and scattered radiation separately using lead shielding" (Xu et al. 2008). However, a chronological view also shows out-of-field dosimetry studies starting from early classical treatment techniques leading to the introduction of more recent IMRT as well as TomoTherapy and stereotactic radiation therapy, ranging from the early 1970s to 2007. It was also noted interestingly, that "Many of these early studies focused on occupational radiation safety (ORS) for medical personnel instead of patient safety and very few reported averaged organ doses" (Xu et al. 2008).

A couple of other works which also attempted to separate leakage and scatter radiation components of out-of-field dose, but with different separation schemes were also noted, "Kase et al. (1983) measured dose from 4 and 8 MV accelerators and a 60Co machine. The group differentiated contributions from leakage and scatter radiation, noting that collimator scatter contributes to about 20–40% of the total dose outside of the treatment field, depending on machine, field size and distance from the field. It was reported that leakage radiation was the major contribution to the out-of-field dose in locations beyond 60 cm from the central axis. Sherazi and Kase (1985) made similar measurements but included the effects of blocks and field wedges. The group found that the use of wedges caused 2–4 times increase in the scattered radiation at any point outside the field" (Xu et al. 2008).

1.4.2 IMRT and Experimental Methods of Out-of-Field Dosimetry study

The literature survey by me also shows that the methods of studying out-of-field dosimetry were predominantly experimental. Meeks et al. (2002) used optically stimulated luminescence dosimeters (OSLD) placed on the sternum and lower abdomen of nine patients to estimate the in vivo absorbed doses as a function of distance from treatment site. The estimated dose was based on irradiation from a 10MV Linac fitted with a dedicated serial TomoTherapy tertiary collimator. These authors concluded, like most of the literature, that it was important to assess the risk of secondary malignancies

from IMRT delivery, and compare this risk against the potential benefits of decreased normal tissue complication probabilities (Meeks et al. 2002).

Vanhavere et al. (2004) used a Rando-Alderson phantom as well as a plexi-phantom in conjunction with an 18MV Varian Linac to make measurements both free-in-air and at different depths in the phantoms, concluding that "when IMRT treatment planning is used, the neutron doses are higher because the number of MU's rises. The gamma part of the effective dose will be slightly lower with IMRT because the organs close to the isocenter will receive less radiation. The organs further away receive a higher dose due to the higher number of MU."

Also Sherma et al. (2006) made two sets of measurements of Out-of-Field point doses under identical conditions, both sets where measured in a plastic phantom with dimensions $35 \times 35 \times 105$ cm^3. One set used previously treated patient specific IMRT beams under sliding window method, of seven patients treated for head and neck and cervical cancer while the other set used dynamic multileaf collimation (DMLC) IMRT fields to simulate static fields with dimensions ranging from 6×6 to 14×22 cm^2 and a 6MV Varian Linac. The two sets of measurements were made with a 0.6cc ion chamber inserted at 5cm depth and placed at 10 points on the same plane as the isocenter, outside the treatment field. In comparing both sets of measurements it was concluded that Out-of-Field dose data generated from uniform DMLC fields can be adopted as baseline data to estimate Out-of-Field critical organ or whole body dose in patients for any clinical sites that were treated by employing the sliding window IMRT technique if appropriate correction factors for field dimensions where applied. Further highlighting the need to improve radiation therapy delivery methods by factoring out-of-field dose data during planning and delivery.

Using a similar approach as Vanhavere et al, Howell et al. (2006) measured photon and neutron doses in a physical phantom, based on IMRT plans of prostate cancer, and focused on calculating effective doses associated with their measurements. They argue that "although IMRT resulted in an increased photon dose to many organs, the data reported herein show that IMRT resulted in an overall decrease in effective dose compared to conventional radiotherapy."

1.4.3 IMRT and Monte Carlo Methods of Out-of-field Dosimetry study

The literature also shows that as measurement data began to build up, methods involving Monte Carlo simulations gained popularity in recent years (Xu et al. 2008). Earlier Monte Carlo studies where based on work by Francois et al. (1988), McParland et al. (1992), and Diallo et al. (1996). Also in more recent work, Kry et al. (2006), realizing how time-consuming measurement based methods are as well as the uncertainty associated with calculated estimations of out-of-field dose data, stated that "MCNPX was used to create a Monte Carlo model of a Varian Clinac 2100 accelerator head operated at 6 MV." In that work, they compared theoretical results from the model and practical results from TLD measurements resulting in an average local difference of 16% (Kry et al. 2006). A more robust attempt was made in a recent study and the authors "expanded and validated our Monte Carlo model for high-energy 18 MV photon therapy, including both photons and neutrons" (Kry et al. 2007b). However they reported average local differences between simulated and measured data for both photon dose to be 17% (1% less than their initial model) and neutron fluences to be 19%.

In the same sense the literature also shows that out-of-field dosimetry studies were carried out for dose reconstruction purposes to enhance the understanding of genetic effects of radiation therapy as well as aid in the development of risk models for particular treatment modalities; "Stovall et al. (2004) reconstructed gonadal dose for childhood cancer patients as part of a multi-institutional effort to study the genetic effects of radiation therapy using methods previously developed (Stovall et al. 1989). Another dose reconstruction project was performed by Stevens et al. (1998) for children who underwent prophylactic cranial conventional radiation therapy. Doses were determined for these children using both anthropomorphic and in vivo measurements. These dosimetry data were then used to improve risk models of thyroid complications to children undergoing similar treatments" (Xu et al. 2008).

Other studies that contribute to the body of work regarding out-of field dosimetry include a report by the American Association of Physicists in Medicine (AAPM) Task Group Report No. 36 (Stovall et al. 2005). Xu et al. (2008) explains that, "This report described dosimetry techniques and data for pregnant radiation therapy patients. Dosimetry data in a slab phantom for locations outside the treatment field were provided

for various beam energies, measurement depths and field sizes. The data were meant to help medical physicists to estimate dose to the fetus before physical measurements are taken.". It is also pointed out that, on the other hand, Kry et al. concluded that "calculations using the TG-36 data can lead to either overestimates or underestimates of the fetal dose for irregular fields " (Xu et al. 2008).

During the period between 1993 and 1997, it is reported that "extensive effort to develop simple and generally applicable methods using measurement data to estimate out-of-field dose was reported by Van Der Giessen and colleagues "(Xu et al. 2008). These works concluded that the contribution to the dose outside the treatment field from radiation leakage and scatter did not differ considerably between treatment machines from different manufacturers (Xu et al. 2008). The literature shows that Subsequent modeling efforts would lead to a recent comparison by Van Der Giessen (1997) between modeled and measured out-of-field dose in patients. For all treatments considered, the calculated dose exceeded the measured dose by about 9% (Xu et al. 2008).

Also, Xu et al. (2008) notes that, by the early 1990s, it was clear that: (1) the photon dose decreases exponentially with increasing distance from the field edge used in the classical modalities; (2) the neutron dose is relatively independent of distance from the field edge; (3) the dependence of photon dose outside the treatment field on both depth and beam energy is very weak; (4) the dependence of neutron dose on depth and beam energy is very strong and (5) the dose outside the treatment field increases with increasing field size. Other key points where noted as follows "The major contributors of dose to tissues in close proximity to the field edge are collimator scatter and patient scatter. As the distance increases from the field edge collimator scatter decreases, and patient scatter becomes more dominant. At greater distances patient scatter and head leakage are approximately equal, and eventually leakage begins to dominate" (Xu et al. 2008).

1.4.4 Out-of-field Dosimetry and Emerging Modalities

As radiation therapy modalities evolve, interest in dose distributions from photon, neutron and protons are becoming apparent in regards to IMRT, TomoTherapy, and

Intensity Modulated Proton Therapy (IMPT) as all these modalities involve beam modulation with monitor units (MU) or radiation outputs greater than classical modalities. This interest is shown by Wroe et al. in a recent contribution to the body of work regarding out-of-field dosimetry in emerging modalities, which concluded that their work "has presented comprehensive dose-equivalent and average quality factor information derived from measured microdosimetric data for various proton treatment configurations and different modalities of primary beam collimation at the Massachusetts General Hospital proton facility" (Wroe et al. 2009). It is also pointed out in the literature, that "With the widespread adoption of Image guided radiation therapy (IGRT) procedures, it makes sense to combine the concomitant and scattered therapy doses in second cancer risk assessment and even in the treatment planning when the imaging dose accounts for several per cents of the therapeutic dose in organs at risk" (Xu et al. 2008).

The extensive literature review by Xu et al. (2008) also lead to the compelling conclusion that encourages further work in out-of-field dosimetry particularly for the evaluation of new treatment modalities, but it is noted that "However, the protection quantity, effective dose, should not be used for absolute risk assessment for specific patient or for epidemiological studies. Instead, organ specific equivalent doses must be used and documented. Therapeutically irradiated populations provide increasingly valuable data for large-scale epidemiological studies on radiation effects involving a wide range of dose levels." This point if further buttressed in a text by Knoll (2002) who states that "Biological effects are not absolute physical quantities that can be measured with high precision. The concept of effective dose or effective dose equivalent is intended only to provide guidance in approximating the potential effects of a given exposure to radiation and should not be regarded as highly accurate or exactly reproducible quantities." Consequently, Xu et al. (2008) encourages that "If collected carefully, dosimetry data for patients can be more accurate (and more relevant because of the well-defined fractionation schemes and well-known radiation field) than those collected for atomic-bomb survivors and workers, thus making it possible to reduce the uncertainty in the derived risk estimates for patients. As the atomic-bomb survivors age eventually cease to be epidemiologically useful, patients irradiated by both therapeutic

and diagnostic imaging procedures will become a critical source of data for continuous refinement of dose–response functions especially in low-level exposures. Such knowledge will in turn allow the radiation oncology community to optimize the radiation treatment procedures."

Xu et al. (2008) concluded that "… majority of the studies focused on determining the so-called out-of-field dose or 'peripheral dose' that are measured in a water phantom at different locations from the edge of the treatment delivery system. Such data are useful in comparing the relative level of secondary radiation from different accelerators or treatment procedures. This type of studies should continue especially for the evaluation of new treatment modalities." Consequently, this conclusion by Xu et al. (2008), in conjunction with two other studies looking at secondary cancer based on epidemiological data, has motivated Trot (2009) to ask:" Can we reduce the incidence of second primary malignancies occurring after radiotherapy?" The author concluded that more research needs to be done to develop new criteria for treatment plan optimization which would include, besides the risk of radiation-induced severe early and late normal tissue damage also the risk of radiation-induced second cancer in the treatment planning process.

Also, like Xu et al. (2008), Trot (2009) points out the importance of improving the treatment planning process to the future of radiation oncology, in particular at a time when new treatment modalities from IMRT and TomoTherapy to IGRT and stereotactic radiosurgery are emerging and taking root in treatment centers. It was noted that, "at present these criteria and models are based on the extrapolation of treatment outcome mostly from outdated therapies. This makes any judgment of the risks of new radiation treatments in individual patients very uncertain if not speculative" (Trot 2009).

These review articles summarized above have identified the important need to generate a diverse data base of out-of-treatment-field dose to healthy organs. This thesis is an effort to add to the existing body of data on out-of-field dosimetry by contributing new data derived from measurements from current IMRT delivery systems as well as out-of-field dose data specific to nasopharyngeal cancer treatment in an anthropomorphic phantom.

1.5 Review of Head and Neck Cancer

This review of head and neck cancer will focus on cancer of the nasopharynx and the use of IMRT in the therapy of NPC. In describing the natural history of carcinoma of the nasopharynx Lee et al. highlights that it frequently arises from the lateral wall, with a predilection for the fossa of Rosenmüller (pharyngeal recess) and the roof of the nasopharynx (Lee et al. 2005). The authors also point out that: 1) tumor may involve mucosa or grow predominantly in the submucosa, invading adjacent tissues including the nasal cavity, although in 5% of patients, tumor extends into the posterior or medial walls of the maxillary antrum and ethmoids, 2) In more advanced stages, tumor may involve the oropharynx, particularly the lateral or posterior wall, 3) Approximately 90% of patients develop lymphadenopathy (disease of the lymph nodes), which is present in 60% to 85% at initial diagnosis. About 50% of patients have bilateral lymph node involvement (Qin et al. 1988), amongst other traits of NPC (Lee et al. 2005). Also worthy of note is the tumor-node-metastasis (TNM) classification which describes the anatomical extent of cancer as highlighted by Greene et al, stating "The objectives of the TNM system are to aid clinicians and investigators in planning treatment, assessing prognosis, stratifying patients for therapeutic studies, evaluating the results of treatment, and facilitating communication" (Greene et al. 2008).

Integral to the management of NPC is the imaging process, computed tomography (CT) and magnetic resonance imaging (MRI), essential to both staging and treatment planning in addition to follow-up of patients (Lee et al. 2005). A Staging system, according to the American Joint Committee on Cancer (AJCC) of the American Cancer Society, is shown on Table 1.1. The literature of NPC shows that prognosis depends on issues such as: epidemiology, stage, cranial nerve involvement, lymph node metastasis, bilateral cervical lymph node involvement, and histology; consequently, because of the anatomical location of the nasopharynx, surgical resection with an acceptable margin is often not achievable, resulting in radiation therapy being the sole treatment for NPC (Lee et al. 2005). This is reflected in the conclusion reached by Geara et al, stating "this study presents strong evidence that the risk of distant metastasis in nasopharyngeal cancer is governed by the extent and level of neck disease which in turn strongly affect disease-specific survival. T-stage and tumor histology are also significant prognostic

indicators for disease-specific survival. T-stage affects survival mainly by its influence on local control, while the impact of histology is through both local control and distant metastasis. Trials investigating the value of adjunctive chemotherapy should probably be restricted to those patients who are at high risk of distant failure. This particularly includes patients with N2-N3 and lower level neck disease" (Geara et al. 1997). However, more recent studies show that as NPC treatment shifts from conformal therapy to IMRT "Lower normal tissue doses and improved target coverage, primarily in the retropharynx, skull base, and nodal regions, were achieved using IMRT. IMRT could potentially improve locoregional control and toxicity at current dose levels or facilitate dose escalation to further enhance locoregional control" (Hunt et al. 2001). But in a similar study done by Wolden et al. following up on their findings that IMRT significantly improves radiation dose distribution over three-dimensional planning for NPC, it was concluded, based on a larger cohort of patients with a longer follow-up time per their first study, that "The pattern of primary site failure within the target volume suggests locally advanced T stage disease may require a higher biologic dose to gross tumor. Rates of severe (Grade 3–4) ototoxicity and xerostomia are low with IMRT as a result of normal-tissue protection. Distant metastases are now the dominant form of failure, emphasizing the need for improved systemic therapy" (Wolden et al. 2006). Furthermore, in a theoretical comparison between more recent radiation therapy methods, intensity-modulated proton therapy (IMPT) and helical TomoTherapy, in the treatment of NPC, Widesott et al. reports that "Excellent target coverage, homogeneity within the PTVs, and sparing of the organs at risk were reached with both modalities. IMPT allows for better sparing of most organs at risk at medium-to-low doses" (Widesott et al. 2008).

Table 1.1 Excerpt (Lee et al. 2005) describing American Cancer Society's Joint Committee on Cancer (AJCC) staging system for Nasopharyngeal Carcinoma. Original print from Green FL's AJCC cancer staging manual, 6th Ed. New York: Springer; 2002.

	AJCC 2002
Primary Tumor	
Tx	Primary tumor cannot be assessed
T0	No evidence of primary Tumor

Tis	Carcinoma in situ
T1	Tumor confined to the Nasopharnyx
T2	Tumor extends to soft tissues of oropharynx and/or nasal fossa
T2a	Without parapharyngeal extension
T2b	With parapharyngeal extension
T3	Tumor invades bony structures and/or paranasal sinuses
T4	Tumor with intracranial extension and/or involvement of cranial nerves, infratemporal fossa, hypopharnyx, orbit, or masticator space
Neck Nodes	
Nx	Regional lymph nodes cannot be assessed
N0	No regional lymph node metastasis
N1	Unilateral metastasis in lymph nodes(s),≤6 cm in gr eatest dimension, above the supraclavicular fossa
N2	Bilateral metastasis in lymph node(s), ≤6 cm in greatest dimension, above the supraclavicular fossa
N3	Metastasis in a lymph node(s):
N3a	> 6 cm in dimension
N3b	Extension to the supraclavicular fossa
Metastases	
MX	Distant metastases cannot be assessed
M0	No distant metastasis
M1	Distant metastasis present

2. Methods

This section elaborates on the methods used to develop IMRT treatment plans for NPC treatment on the TRILOGY and TOMOTHERAPY radiation therapy delivery systems. Also outlined is the use of TLD-100 chips to measure Out-of-field-dose due to secondary scatter radiation in the phantom and leakage radiation from the treatment machine, arising as a result of NPC therapy in the ATOM phantom.

2.1 Simulation of the Atom® Phantom

In this study, a full scan of the Adult Male ATOM phantom was done using a Siemens Emotion single-slice CAT Scan, Computed Tomography (CT) machine, generating 3mm thick CT slices with a resolution of 1mm×1mm pixels (picture elements) and subsequently reconstructing the slices to 906, 1mm-thick, CT slices of the phantom Fig 2.1 The CT images where then exported to the Varian Eclipse treatment planning system, where a three dimensional (3D) image of the head and neck (H&N) region Fig 2.2, was generated and used in the treatment planning process.

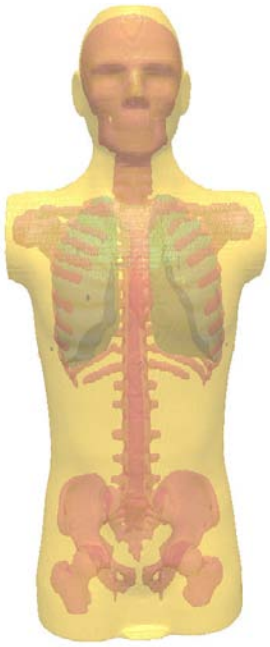

Figure 2.1 Image of Atom phantom generated from 906 CT slices, showing the bone, soft tissue and lung tissue, as designed by CIRS Tissue Simulation Technology.

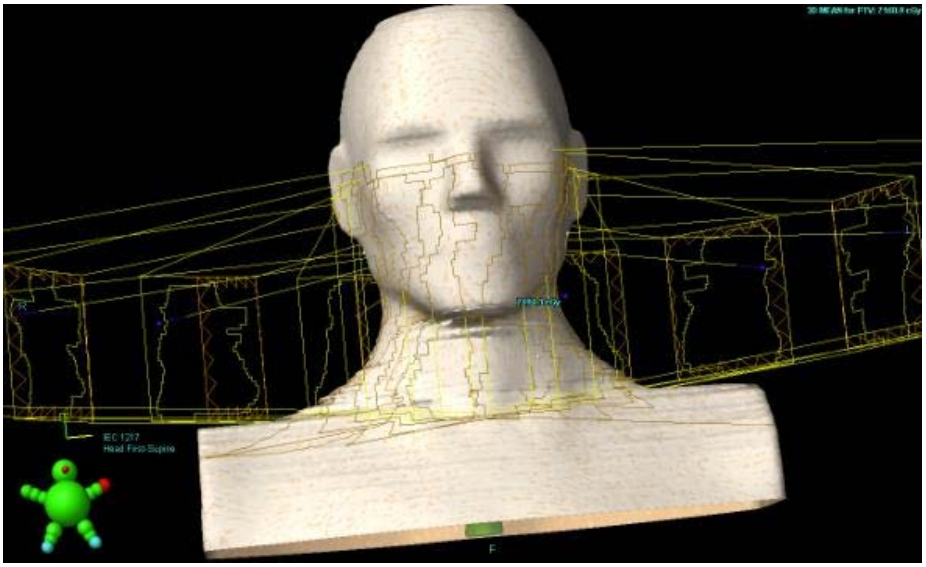

Figure 2.2 3D-Image of Head and Neck Region of Atom generated from CT images imported to the Varian Eclipse Treatment Planning System. Simulated Fluence patterns of intensity modulated beams entering and leaving the phantom are also shown in the image of the phantom.

2.1.1 Segmentation of the ATOM® Phantom

A three dimensional imaging, modeling and measurement software (3D-Doctor), by Able Software Corporation, was used to segment the CT images of the ATOM phantom. The CT images where imported to 3D-Doctor in their 2D DICOM file format and saved as a 3D TIFF (Tagged Image File Format) file. Three object-boundaries where then created for the body (Soft Tissue, Spinal Cord, Spinal Disks, and Brain), lungs and adult bone of the phantom. The boundaries where defined base on the phantom material specifications shown on Table 2.1.1.The soft tissue, spinal cord, spinal disk and brain where all grouped under the body-object due to the similarity of their density specification in the phantom.

3D-Doctor was then used to segment the three objects on all image slices by mapping the range of pixel values in each object to a single value for each of the 3 objects (Body, Lungs and Adult Bone). The segmented 3D image was then saved as a RAW (raw data) file, shown graphically on Fig 2.3

Table 2.1.1 Excerpts from the CIRS Manual - Phantom Material Specifications

	Physical Density (g/cc)	Electron Density (g/cc)
Adult Bone	1.60	5.030×10^{23}
Soft Tissue	1.05	3.434×10^{23}
Spinal Cord	1.07	3.448×10^{23}
Spinal Disks	1.15	3.694×10^{23}
Lungs	0.21	0.681×10^{23}
Brain	1.07	3.470×10^{23}

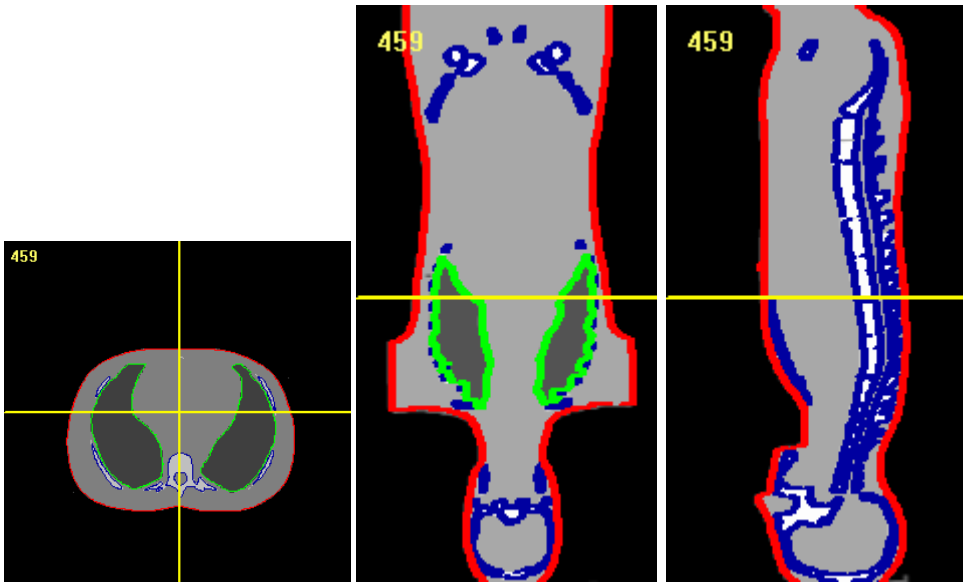

(a) Axial View (b) Coronal View (c) Sagittal View

Figure 2.3 Three views of the segmented Adult Male ATOM phantom generated using the 3D-Doctotr Software. Images show the Adult Bone in white surrounded by blue boundary contours, Soft Tissue in dark-gray surrounded by red body-boundary contours, and lung in light-gray surrounded by green boundary contours. The yellow lines across (b) the coronal and (c) sagittal views indicate the 459th slice shown on (a) the axial view. The vertical yellow line on (a) the axial view shows the location of (c) the sagittal view. The horizontal line on (a) the axial view shows the location of (b) the coronal view.

2.2 Treatment Planning

The core of IMRT is in the treatment planning and optimization process (Dong et al. 2005). This process starts with the delineation of the gross target volume, the CTV and the critical normal structures knows as OAR's and ends with the translation of clinical requirements for a specific clinical problem into machine deliverable commands (Dong et al. 2005). The effectiveness of IMRT is contingent on the precision of the delineation process.

IMRT plans can be created using either the "forward planning" or the "inverse planning" method (IMRT-CWG 2001) as depicted on Figure 2.4. The forward-planning method requires planners to first specify beam directions, shapes and intensities before the computer calculates the resulting dose distributions. Planners then manually adjust beam directions, beam shapes and beam intensities on the basis of their planning experience and intuition (Xia 2005). On the other hand, the inverse-planning method starts with a desired dose distribution and ends with fluence distributions that when taking together, approximate the desired dose distribution (Brahme 1988). Xia points out that, "the main differences between forward planning and inverse planning are that the plan quality is evaluated by a score rather than by the planner's intuition and that the number of parameters adjusted by the computer is extremely large in inverse planning" (Xia 2005).

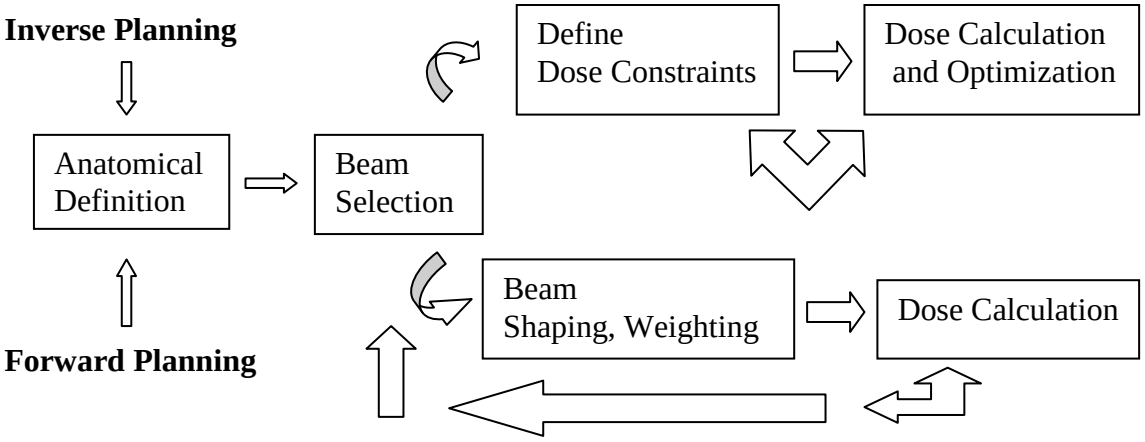

Figure 2.4 Flow chart for both forward and inverse planning processes.

2.2.1 Treatment Planning on Varian's Eclipse™ and IMRT of Head and Neck Cancer on the Varian Clinac (TRILOGY)

In this work, the first treatment plan was derived on the Varian Eclipse external beam treatment planning software by adopting the inverse-planning process based on Radiation Therapy Oncology Group (RTOG) protocols (RTOG 0225). The prescription dose was 70 Gy and the plan was to deliver 100% of the prescription dose to 95% of the target volume – PTV. The adult male ATOM phantom has no defined organs; therefore the first step was contouring of OAR representative of a typical IMRT of NPC case. The OAR to be contoured was chosen based on typical NPC cases at the Vassar Brothers Medical Center in Poughkeepsie NY. These organs are: spinal cord, brain stem, left parotid gland, right parotid gland, mandible, globe, optic nerve, optic chiasm, lens, middle ear, glottic larynx, pituitary gland and skin. Contours where delineated on each relevant CT slice of the H&N region of the atom phantom and visualized in 3D as shown in Figure 2.5 to ensure good representation of normal organs in H&N region of a typical patient.

The next step was the contouring of two tumor targets representing a high dose target called PTV located in the nasopharynx and a lower dose target called "PTV59 – PTV" which encompassed additional lymph nodes contoured as nodal chains on the lateral sides of the neck region at risk of disease spread. Patient positioning and tumor target uncertainties where factored into the contouring process resulting in a 2cm margin around the centrally-located primary-GTV. Both tumor target volumes are shown as red and blue respectively in Fig 2.5 (a) and (b). The treatment goal for this work was to deliver a dose of 70 Gy to more than 95% of PTV and a dose of 59.4 Gy to more than 95% of PTV59-PTV simultaneously. This goal was based of standards of judging IMRT treatment plans for an advanced case of NPC (RTOG 0225 2009). Also the acceptable dose to OAR was based of dose constraints of a typical NPC case at Vassar Brothers Medical Center in Poughkeepsie NY.

Consequently, the plan was started using a 7-field beam arrangement for NPC treatment (Hunt et al. 2001). The dose constraints where then entered into Eclipse to steer the inverse planning system towards the desired treatment plan. A systematic trial and error approach, said to be the only way to "…find a compromise between the dose

coverage of the tumor volumes and the sparing of the sensitive structures" (Xia 2005), was used to find a compromise treatment plan. The compromise plan ended up with an 8-field beam arrangement – shown on Figure 2.2, in order to achieve acceptable coverage of the two tumor volumes as well as spare OAR. Coverage of the tumor volumes and sparing of the OAR based on the final 8-field treatment plan achieved with Eclipse is depicted graphically on Figure 2.6.

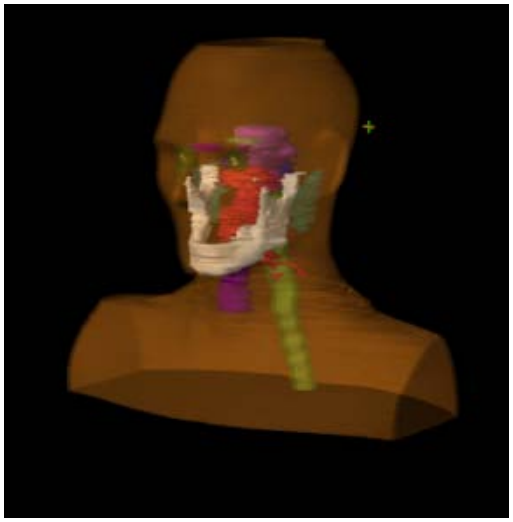

(a)

(b)

(c)

Figure 2.5 A 3D view of the contoured OAR in the H&N region of the ATOM, using the Varian Eclipse treatment planning software. (a) Anterior Posterior (AP) view with the OAR and High Dose Gross Tumor PTV in Red. (b) AP view with the OAR and Lower Dose Clinical Target Volume named "PTV59-PTV" in Blue encompassing the nodal chains on each side of the neck region. (c) PA view.

Once the plan was completed on the Eclipse treatment planning software, a statistical report showing the maximum, minimum and mean doses as well as percentages of the volume associated with the dose coverage, along-side a dose volume histogram (DVH) , was generated for plan evaluation and comparison - with planning goals for the tumor volumes and dose constraints for OAR. Table 2.2.1 shows the dose-constraint goals for OAR, and Fig 2.7 shows the DVH and statistical report generated for the 8-field NPC IMRT treatment plan on Eclipse. Additionally, as the dose distribution criteria was met, the dose displayed on each CT slice was examined for hot and cold spots corresponding to over an under dosed areas. In one trial a dose limiting structure was simulated to better improve dose coverage, to a hot spot found close to the left parotid gland, to achieve the final dose distribution of the plan. Fig 2.8 shows a CT slice depicting dose coverage using isodose lines. The final plan to deliver the prescription of 7000 cGy at 200 cGy/fraction for 35 fractions resulted in the monitor unit (MU) linac-output of 1073 MU/fraction for the NPC IMRT treatment using TRILOGY.

Table 2.2.1 Dose Constraints and Goals of OAR in a NPC IMRT plan for a clinically relevant case gotten from Vassar Brothers Medical Center in Poughkeepsie. Dmax is equivalent to "Maximum allowed dose to organ at risk", D50 is equivalent to 50% of the volume allowed to be covered by dose, and D66 is equivalent to 66% of volume allowed to be covered by dose.

Organ At Risk	Goal (cGy)
Cord + 5mm (Dmax)	4500
Brain Stem + 5mm (Dmax)	5500
Ipsi. Parotid (D50)	3000
Contra. Parotid (D50)	2400
Mandible (Dmax)	6000
Globe (Dmax)	4500
Optic Nerve + 2mm (Dmax)	5000
Optic Chiasm +2mm (Dmax)	4500
Lens +2mm (Dmax)	500
Middle Ear	5000
Glottic Larynx (D66)	5000
Pituitary (D50)	2060
Skin (Dmax)	5300

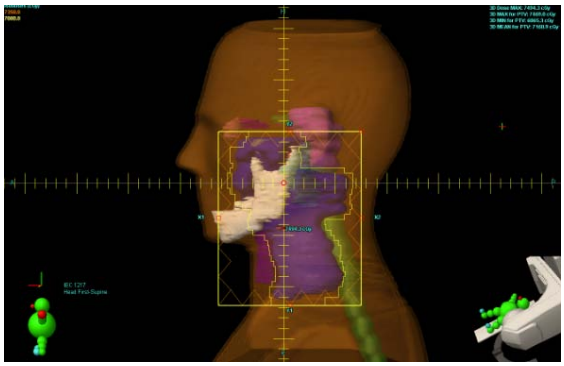

(a) LO – 90 degrees

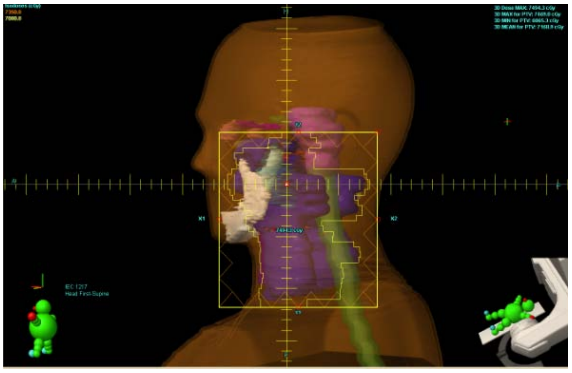

(b) LAP – 115 degrees

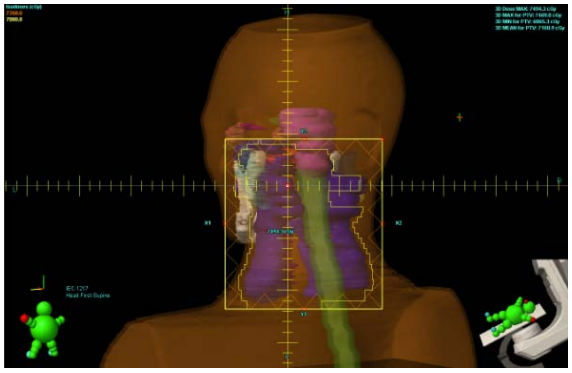

(c) LAP – 140 degrees

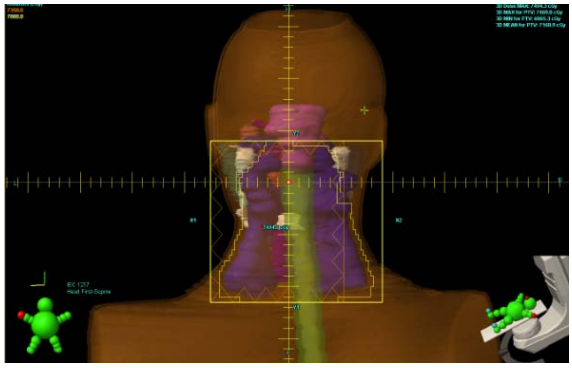

(d) LAP – 165 degrees

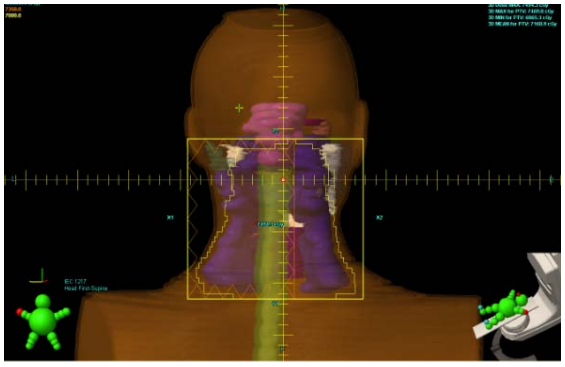

(e) RAP – 190 degrees

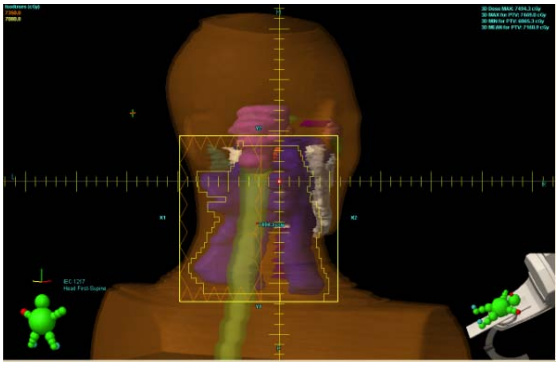

(f) RAP – 215 degrees

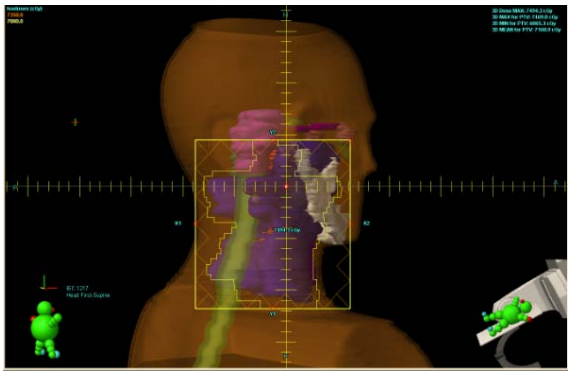

(g) RAP – 240 degrees

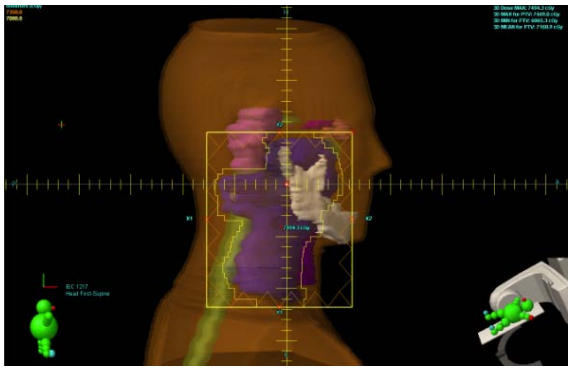

(h) RAP – 260 degrees

Figure 2.6 Eclipse Graphical 3D representation of the 8-fields of the NPC IMRT treatment plan showing the fluence pattern as well as the organ spearing on each field of view - LO (Left Orthogonal Field), LAP (Left Anterior Posterior Field), RAP (Right Anterior Posterior Field) , and respective angles of beam entry.

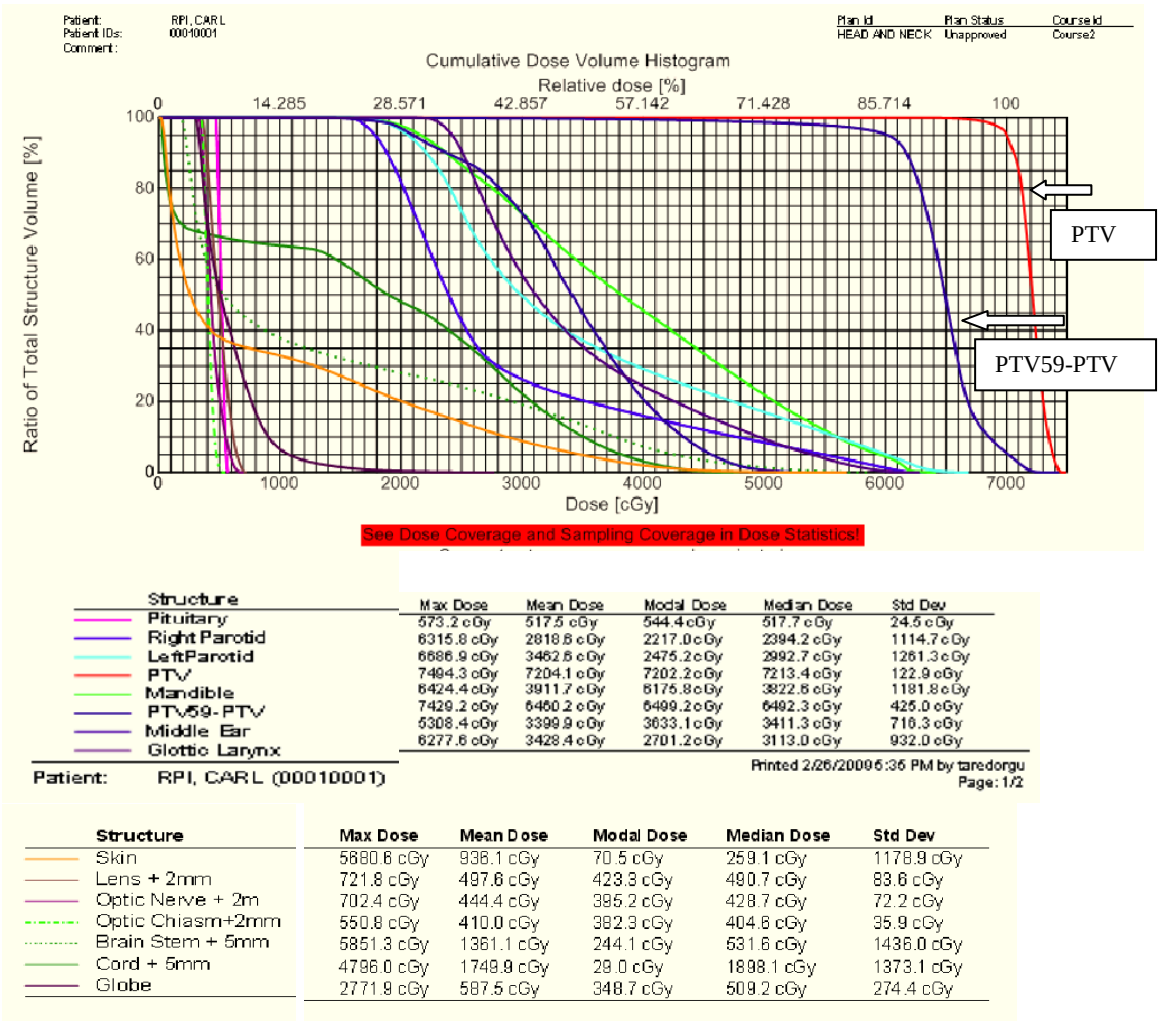

Structure	Max Dose	Mean Dose	Modal Dose	Median Dose	Std Dev
Pituitary	573.2 cGy	517.5 cGy	544.4 cGy	517.7 cGy	24.5 cGy
Right Parotid	6315.8 cGy	2818.6 cGy	2217.0 cGy	2394.2 cGy	1114.7 cGy
LeftParotid	6686.9 cGy	3462.6 cGy	2475.2 cGy	2992.7 cGy	1261.3 cGy
PTV	7494.3 cGy	7204.1 cGy	7202.2 cGy	7213.4 cGy	122.9 cGy
Mandible	6424.4 cGy	3911.7 cGy	6175.8 cGy	3822.6 cGy	1181.8 cGy
PTV59-PTV	7429.2 cGy	6460.2 cGy	6499.2 cGy	6492.3 cGy	425.0 cGy
Middle Ear	5308.4 cGy	3399.9 cGy	3633.1 cGy	3411.3 cGy	716.3 cGy
Glottic Larynx	6277.6 cGy	3428.4 cGy	2701.2 cGy	3113.0 cGy	932.0 cGy

Patient: RPI, CARL (00010001)
Printed 2/26/2009 6:36 PM by taredorgu
Page: 1/2

Structure	Max Dose	Mean Dose	Modal Dose	Median Dose	Std Dev
Skin	5680.6 cGy	936.1 cGy	70.5 cGy	259.1 cGy	1178.9 cGy
Lens + 2mm	721.8 cGy	497.6 cGy	423.3 cGy	490.7 cGy	83.6 cGy
Optic Nerve + 2m	702.4 cGy	444.4 cGy	395.2 cGy	428.7 cGy	72.2 cGy
Optic Chiasm+2mm	550.8 cGy	410.0 cGy	382.3 cGy	404.8 cGy	35.9 cGy
Brain Stem + 5mm	5851.3 cGy	1361.1 cGy	244.1 cGy	531.6 cGy	1436.0 cGy
Cord + 5mm	4786.0 cGy	1749.9 cGy	29.0 cGy	1898.1 cGy	1373.1 cGy
Globe	2771.9 cGy	587.5 cGy	348.7 cGy	509.2 cGy	274.4 cGy

Figure 2.7 DVH and excerpts of the statistical report from the Eclipse treatment planning software used to develop the 8-field NPC IMRT treatment plan for TRILOGY.

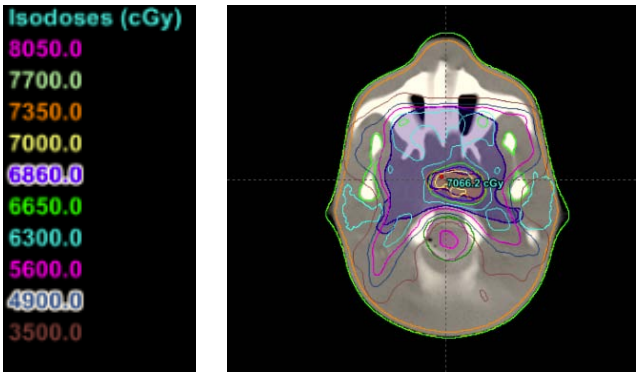

Figure 2.8 Excerpts from an Eclipse treatment plan analysis screen shot showing a transverse cross sectional 2D CT slice with Isodose lines representing dose coverage based on the NPC IMRT 8-field Treatment plan that was developed.

Once the treatment plan was approved, all the CT images used for planning was exported to the MOSAIQ software used to check and confirm field setup, set and confirm beam-on time and verification of the treatment Isocenter and spatial positioning of the couch to ensure it corresponds with specifications of the treatment fields before final treatment delivery on the TRILOGY Linac. Final treatment delivery was done using two ATOM phantom treatment-setup configurations: 1) with all the transverse cross sectional slices of the Adult Male ATOM® phantom intact. 2) Without the transverse cross sectional slices in the region representing the PTV. The treatment setups are shown on Figure 2.9. The adequate number of cross sectional slices to remove was based on simulation of beam entry and exit points using Eclipse to depict a 3D view of the irradiation process as shown of Figure 2.10. Styrofoam blocks, which have an electron density value similar to air, where then used to replace the physical crossectional slices in order to reduce the production of in- phantom scatter radiation to negligible levels as shown on Figure 2.9b. Also a Kilovoltage Cone Beam CT (KVCBCT) imaging feature of the TRILOGY was used to generate and examine treatment position accuracy to ensure there was no positional shift in the treatment setup, mimicking an actual clinical situation, as shown of Figure 2.11.

(a)

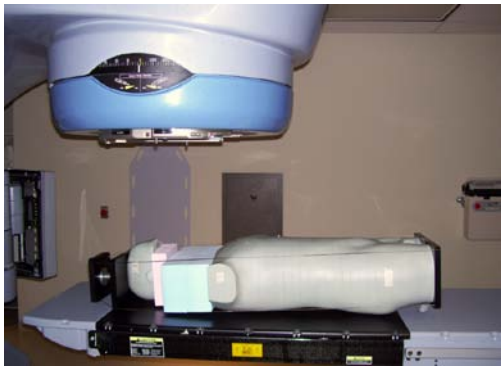

(b)

Figure 2.9 Adult Male ATOM® (a) with all the transverse cross sectional slices of the phantom intact (Congiguration-1) for IMRT of NPC using TRILOGY. b) With the transverse cross sectional slices replaced with Styrofoam blocks (Configuration-2) to simulate air and reduce in-phantom scatter to negligible levels in the region representing the Planning Treatment Volume (PTV) under same treatment conditions as part-a.

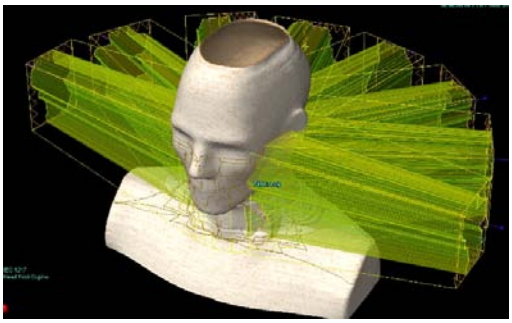

Figure 2.10 Eclipse simulation of Beam-Entry and Beam-Exit points as seen below the beams in the shoulder region, to enable adequate replacement of phantom slices with Styrofoam material during treatment delivery, enabling the reduction of in-phantom scatter radiation to organs out-of-field, for one of the two treatment-setup configurations.

(a)

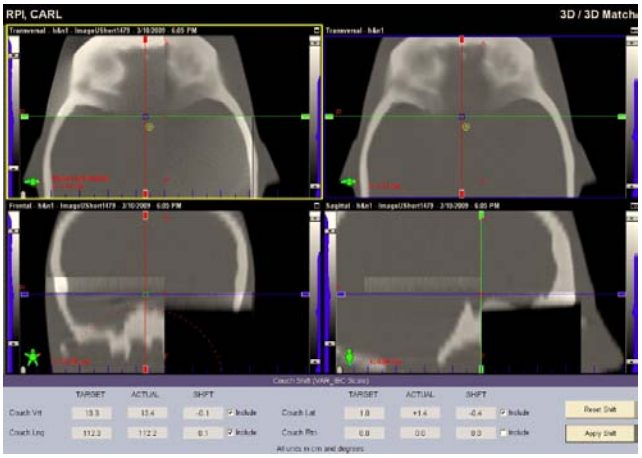

(b)

Figure 2.11 KVCBCT On board imaging of the ATOM phantom before receiving IMRT of NPC on the TRILOGY. (a) Configuration with all slices of the phantom in place, showing a good match between treatment-planning image (dark shade) and treatment-position image (light shade) superimposed. (b) Configuration with in-field slices replaced with Styrofoam blocks. The 4th quadrant can be seen as air equivalent confirming good representation of air equivalent electronic density.

2.2.2 Treatment Planning and IMRT of Head and Neck on TomoTherapy® Hi-Art® II system

In this work the second treatment plan was developed using the TomoTherapy Hi-Art II system (TOMO). Like the Eclipse system, the same prescription of 95% of PTV volume receiving at least 7000 cGy in 35 fractions was also set for TOMO. All images and contoured regions that was developed in the Eclipse planning system was exported to TOMO eliminating the need to generate contours and also ensuring uniformity in the images used for planning and eventual comparison of treatment outcomes(in terms of Out-of-Field dose to organs) due to the different treatment plans developed using different systems.

With the images uploaded in TOMO, the treatment planning commenced with the setting of the same dose constraints used to develop the Eclipse plan. The TOMO system, using inverse-planning, was then tasked to meet the dose constraints. Trial and error was also adopted while developing the TOMO plan, and priorities were adjusted to first meet the dose to PTV and PTV59-PTV. Subsequently the priority was increased to meet minimum dose levels to OAR. The DVH showing the dose coverage to the target volumes and OAR is depicted on Figure 2.12. Three different views of dose coverage on the CT images are also shown on Figure 2.13 for plan analysis purposes. The treatment

setup of both configurations using TOMO, similar to the treatment with TRILOGY, is depicted on Figure 2.14. Unlike TRIROLOGY's KVCBCT, TOMO uses a Megavoltage CT (MVCT) as an on-board imager for treatment setup verification. Figure 2.15 shows results of treatment setup verification using the MVCT in TOMO. The final plan to deliver the prescription of 7000 cGy at 200 cGy/fraction for 35 fractions resulted in a treatment time of 820.9 seconds/fraction for the NPC IMRT treatment using TOMO.

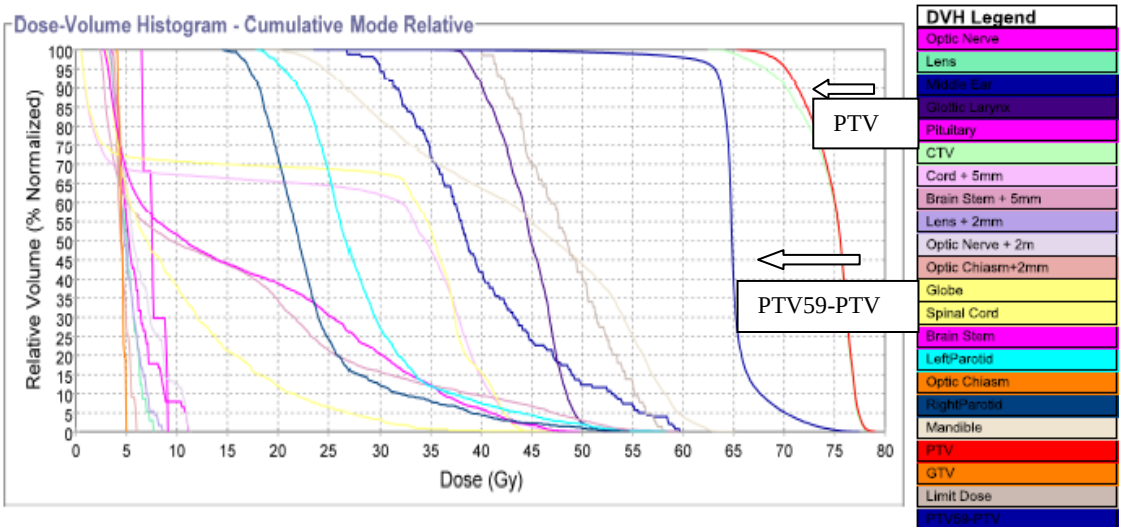

(a)

Tumor Constraints

Name	Blocked	Use?	Importance	Overlap Priority	Max Dose Constr. [Gy]	Max Dose Pen.	DVH Vol [%]	DVH Dose [Gy]	Min Dose Constr. [Gy]	Min Dose Pen.	Max Dose [Gy]	Min Dose [Gy]	Median Dose [Gy]	Avg Dose [Gy]	StdDev Dose [Gy]	Physical Vol [cc]
PTV	None	yes	100	1	70.00	100	95.00	70.00	70.00	100	78.96	59.95	75.57	74.83	2.27	63.07
PTV59-PTV	None	yes	80	2	59.40	80	95.00	59.40	59.40	80	77.65	23.73	64.93	65.22	2.98	498.25

Sensitive Structure Constraints

Name	Blocked	Use?	Importance	Overlap Priority	Max Dose Constr. [Gy]	Max Dose Pen.	DVH Vol [%]	DVH Dose [Gy]	DVH Pt. Pen	Max Dose [Gy]	Min Dose [Gy]	Median Dose [Gy]	Avg Dose [Gy]	StdDev Dose [Gy]	Physical Vol [cc]
Optic Nerve	None	yes	95	9	50.00	95	5.00	50.00	95	11.17	3.53	5.32	6.06	2.11	0.52
Lens	None	yes	95	14	5.00	95	2.00	5.00	95	7.71	3.34	5.22	5.14	1.13	0.20
Middle Ear	None	yes	100	15	40.00	100	5.00	35.00	100	59.71	26.91	38.50	40.17	7.72	2.18
Glottic Larynx	None	yes	95	11	51.00	95	66.00	50.00	95	55.71	36.46	44.89	44.69	3.12	25.04
Pituitary	None	yes	95	12	20.70	95	50.00	20.60	95	9.13	6.55	7.66	7.71	0.96	0.13
Skin		no								65.34	0.29	2.53	12.99	15.73	771.69
CTV	None	yes	60	18	74.00	60	5.00	74.00	60	78.94	62.60	75.60	74.51	2.87	36.98
IMRT PV 1		no								0.00	0.00	0.00	0.00	0.00	0.00
Cord + 5mm	None	yes	95	2	43.00	95	5.00	43.00	95	46.80	0.56	34.53	25.11	16.85	74.70
Brain Stem + 5mm	None	yes	95	8	55.00	95	5.00	55.00	95	60.12	2.32	9.65	15.79	14.54	50.51
Lens + 2mm	None	yes	95	20	5.00	95	2.00	5.00	95	8.59	3.49	4.82	5.14	1.28	0.74
Optic Nerve + 2m	None	yes	95	10	50.00	95	5.00	50.00	95	11.22	3.43	5.51	6.33	2.26	1.43
Optic Chiasm+2mm	None	yes	95	6	45.00	95	2.00	45.00	95	6.04	3.79	4.46	4.66	0.66	2.17
PTV59.4		no								78.53	29.91	64.92	65.22	2.77	497.93
Globe	None	yes	95	22	45.00	95	5.00	45.00	95	47.32	2.81	7.29	10.37	7.89	7.60
Spinal Cord	None	yes	95	1	45.00	95	5.00	45.00	95	44.56	0.59	35.43	26.49	16.38	31.75
Brain Stem	None	yes	95	7	55.00	95	5.00	55.00	95	49.65	2.73	10.93	16.45	13.25	33.27
BODY		no								78.96	0.29	1.41	11.56	19.29	8,143.85

(b)

Figure 2.12(a) DVH and (b) excerpts of the statistical report from the H-Art II treatment planning software used to develop the 8-field NPC IMRT treatment plan for TOMO.

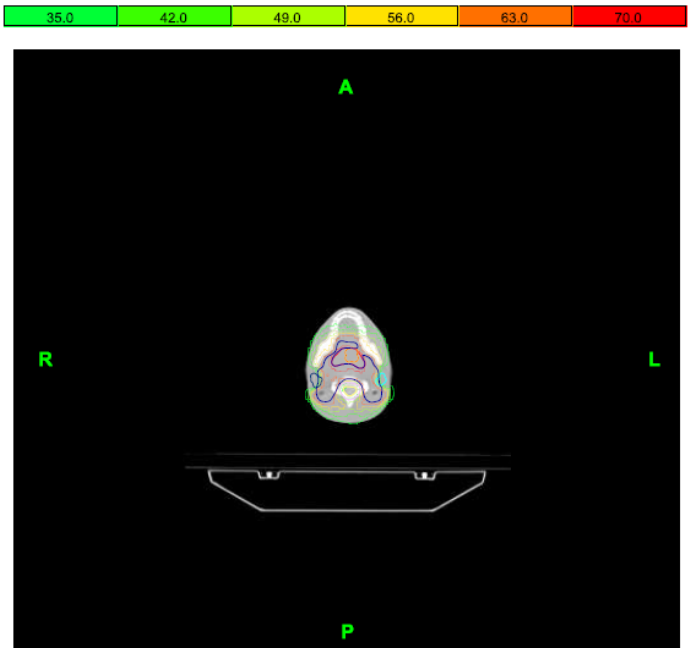

(a) Transverse Cross Sectional View

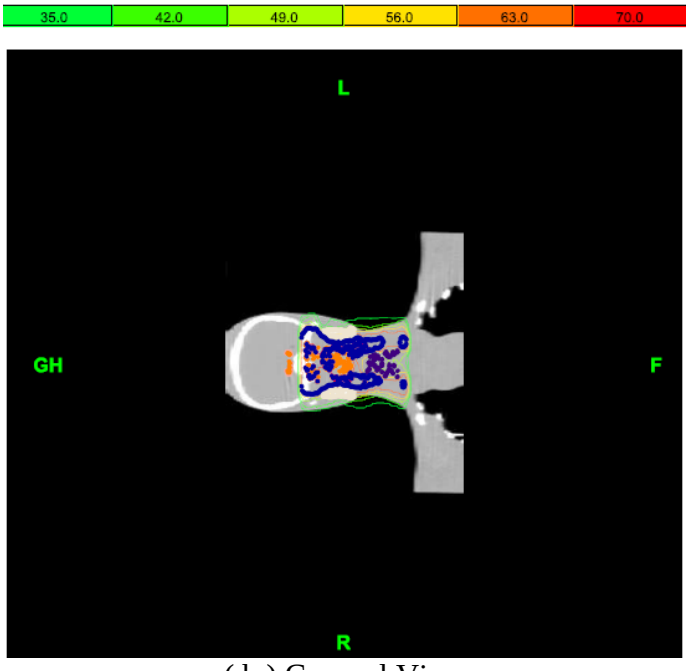

(b) Coronal View

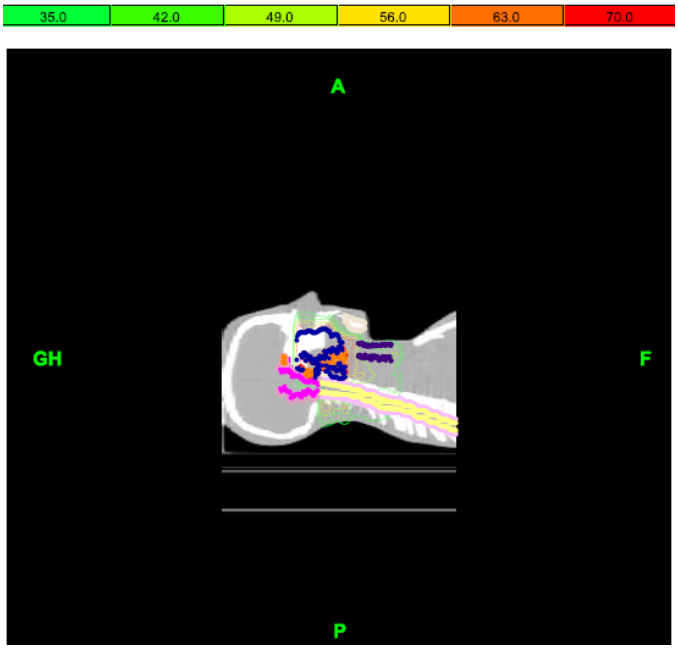

(c) Sagittal View

Figure 2.13 Excerpts from a TOMO treatment plan analysis screen shot showing the Isodose legends above (a) transverse cross sectional 2D CT slice with Isodose lines representing dose coverage based on the NPC TOMO Treatment plan (b) Coronal view of same image. (c) Sagittal View of the same image.

(a)

(b)

Figure 2.14 Adult Male ATOM® phantom being set up for Out-of-Field organ dose measurements on TLDs placed in vivo (a) with all the transverse cross sectional slices of the phantom intact (Configuration-1) for IMRT of NPC using TOMO. b) With the transverse cross sectional slices replaced with Styrofoam blocks (Configuration-2) to simulate air and reduce in-phantom scatter to negligible levels in the region representing the Planning Treatment Volume (PTV) under same treatment conditions as part (a)

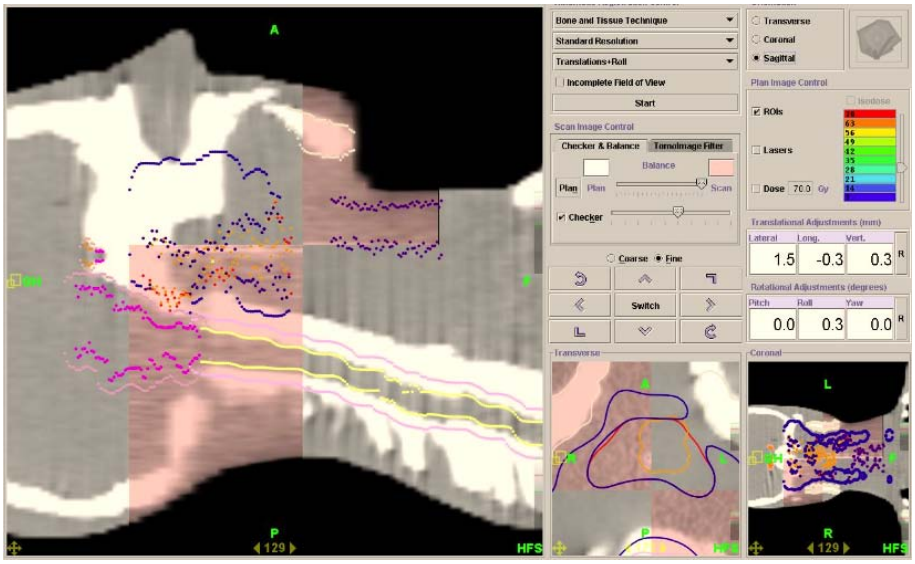

Figure 2.15 A view of MVCT image from the TomoTherapy® Hi-Art® treatment planning system, of the ATOM phantom taken before receiving IMRT of NPC for both configurations, as described previously, of the experiment. The large Image shows the sagittal view of MVCT in pink, superimposed on the planning CT image showing good alignment before treatment. The next small image is the transverse view of the same image and the last image is the coronal view.

2.3 Thermo-luminescence Dosimeter (TLD) Calibration & Measurements

TLD-100 chips were found to be a suitable detector for measuring out-of-field dose for radiation therapy treatment energies up to and including 10MV (Kry et al. 2007a). Thus in this work TLD-100 chips from Harshaw Chemical Company, Solon, OH, with similar sensitivities where selected by exposing a number of chips to a dose rate of 300 mR/min with a ^{137}Cs gamma-ray source, and subsequently annealing the chips with the TLD reader to determine 200 chips with similar sensitivities. The TLD-100 chips were then calibrated against a National Institute of Standards and Technology (NIST) traceable Victoreen Condenser "R" ion chamber-measurements using a Cs-137 gamma-ray source. The appropriate calibration factors for the measurement instrument, temperature and pressure where used to determine that the average dose rate of the gamma source was (15.055$\pm$ 0.001) mR/min at 80-cm distance with no lead shielding. A calibration curve of dose (mRem) versus nanoCoulomb (nC) output was generated as shown on Fig 2.16.

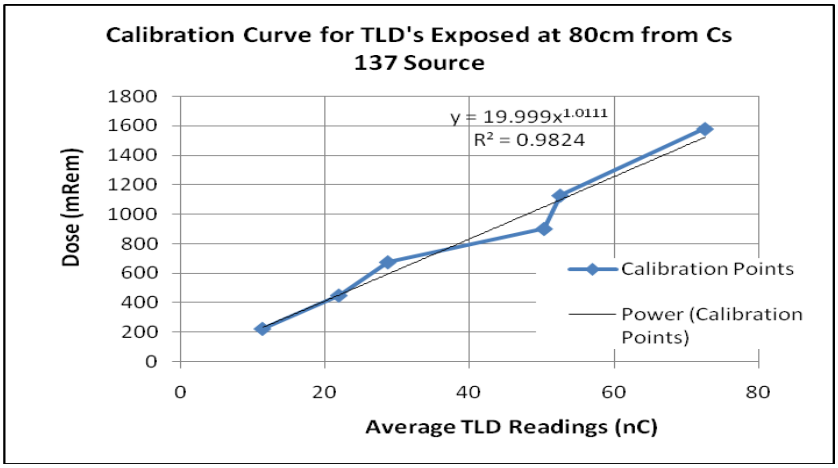

Figure 2.16 Calibration Curve generated using a NIST traceable Condenser "R" Chamber at RPI placed at 80 cm from a Cs-137 gamma point source, and then varying the exposure time to establish calibration points. The power calibration points were generated using excel software as a power regression line of best fit through the established calibration points with the associated R^2 regression coefficient shown on the chart.

These chips were then placed at 15 predetermined measurement points in the anthropomorphic ATOM phantom for a set of measurements. A total of 4 sets of measurement resulting in 60 measurements where conducted for this study. The 4 set of measurements corresponds to a one-fraction delivery of IMRT for NPC (2 sets each for TRILOGY and TOMO for the two configurations described earlier). The location of the measurement points are outlined in the following listing of corresponding number of measurement points in each organ that was studied: the brain –two points, esophagus – 2 points, lung – two points, liver – two points, stomach – two points, kidneys – two points, prostate – two points, bladder – one point, and testes – one point. At each measurement point, 3 TLDs were positioned one above the other to capture 3 measurement reading within the location which would enable the computation of an average dose to each measurement point in all the organs of interest.

3. Results and Discussion

The TLD measurement data which was the basis for the Out-of-Field organ dose was analyzed and adjusted for background reading using the formula;

TLD point Readings (nC) – TLD Background (nC) = Net TLD Readings (nC) ***(1)***

There was an 8% relative error in the average background measurements used to adjust all the TLD readings. Conversion of TLD readings to corresponding photon point doses based on the determined dose rate of (15.055± 0.001) mR/min at 80-cm distance was enabled by the calibration plot which reflected the functional relationship between photon dose and average TLD readings. Thus after applying a quality factor of one for gamma ray photons as well applying a conservative conversion factor of one, from mR to mRem, we arrived at the following calibration-curve conversion-equation:

$$\textbf{Dose (mRem)} = 19.999 \times \textbf{Average TLD Readings (nC)}^{1.0111} \quad (2)$$

Based on equation 2, the Out-of-Field organ doses' and dose-contributions as a result of leakage and scatter radiation where computed. This measured leakage radiation and computed scatter radiation component of Out-of-Field organ dose was achieved due to the treatment-configuration setups (Configuration-1 and Configuration-2) shown in earlier sections, for IMRT of NPC on the TRILOGY and TOMO external beam radiation delivery systems, which were used in this work.

The relative errors in the measured TLD values used for organ dose computations ranged from 1.47 – 34.4% and 5.39 – 17.37% in the TRILOGY (with slices intact and removed respectively). Likewise, 3.05-34.83% and 5.69-35.64% in TOMO (with slices intact and removed respectively) as listed in Tables 3.0 and 3.1. The propagated uncertainty for the organ dose values ranged from 8.01-32.59 % in the lungs and testes respectively for TRILOGY and 6.01-41.35% in the kidneys and lungs respectively for TOMO computations. The associated propagated errors for the organ dose computations where derived using the propagated error of the mean standard deviation of the net TLD readings in all measurement points per organ using the following formula.

Organ Dose Propagated Error = 1.0111 × (Error propagated in Average Net TLD Readings per Organ/ Average Net TLD readings per Organ) ***(3)***

Where the value 1.0111 is associated with the power of the calibration curve derived to convert TLD nanocolumb readings to organ dose in mRem.

Propagated error values are shown for the corresponding organs, in Tables 3.0 and 3.1. In regards to equivalent dose to organs out-of-field, the radiation weighting factor as published by the ICRP publication 60 and reappraised in ICRP publication 92, gives the photon a radiation weighting factor of one. Consequently "…The resulting weighted dose is designated as the organ- or tissue-equivalent dose, H_T" (ICRP 2003). As a direct consequence the calculated and graphed organ doses shown in sections 3.1 and 3.2 can also be looked at as Out-of-Field equivalent organ doses in units of Sieverts. The organ dose normalized to MU for TRILOGY and treatment-time for TOMO was also graphed for comparison because of the similar importance attached to minimizing MU in the final treatment-plan for TRILOGY as well as the importance attached to minimizing treatment-time in the final treatment-plan for TOMO – Fig 3.16. The MU which represents the output of the Varian Clinac was 1cGy/MU as calibrated by the cancer center. The Atom phantom measurements represented one fraction of the prescribed 35 fraction clinical treatment of NPC at the Dyson Cancer Center in Poughkeepsie New York, which would deliver a dose of 7000cGy to the planning target volume (PTV)

Table 3.0 Relative errors in TLD point measurements used to compute Out-of-Field Organ Doses from IMRT of NPC using TRILOGY. The last column shows the associated Propagated-Errors in the resulting computed Out-of-Field Organ Doses.

Organs	**Relative error in TLD Point readings with Slices (Configuration-1)**	**Relative error in TLD Point readings with slices removed (Configuration-2)**	**Error Propagated in Organ Dose**
Brain	8.98%	5.53%	13.70%
	9.78%	7.60%	
Lungs	1.47%	9.39%	8.01%
	10.07%	9.86%	
Esophagus	5.95%	8.38%	12.15%
	15.76%	14.65%	

Liver	4.36%	8.85%	17.07%
	16.61%	5.39%	
Stomach	34.24%	14.99%	31.53%
	5.66%	9.11%	
Kidneys	5.52%	10.68%	16.57%
	13.54%	16.21%	
prostate	21.55%	11.66%	21.79%
Bladder	11.26%	10.73%	11.38%
Testes	32.23%	17.37%	32.59%

Table 3.1 Relative errors in TLD point measurements used to compute Out-of-Field Organ Doses from IMRT of NPC using TOMO. The last column shows the associated Propagated-Errors in the resulting computed Out-of-Field Organ Doses.

Organs	**Relative error in TLD Point readings with Slices (Configuration-1)**	**Relative error in TLD Point readings with slices removed (Configuration-2)**	**Error Propagated in Organ Dose**
Brain	13.91%	8.66%	12.79%
	4.95%	12.40%	
Lungs	5.20%	18.78%	7.12%
	3.05%	11.94%	
Esophagus	11.07%	39.34%	17.65%
	13.07%	5.69%	
Liver	3.29%	17.67%	13.26%
	13.63%	22.28%	
Stomach	6.22%	36.01%	41.35%
	34.83%	12.34%	

Kidneys	4.17%	15.87%	6.01%
	4.22%	9.33%	
Prostate	7.81%	15.13%	7.90%
Bladder	11.41%	12.76%	11.53%
Testes	17.08%	6.93%	17.27%

3.1 Head and Neck IMRT Out-of-Field Organ and Equivalent Dose Results from Varian Clinac (TRILOGY)

In this section a graphical presentation is given of the measurements and computations of Out-of-Field organ dose specific to the Varian Clinac – TRILOGY delivery system. It is noted that because the operational energies of the delivery systems was 6MV , only the photon dose component of Out-of-Field dose is considered in this study. Thus, organ doses are also equivalent doses in units of Sieverts due to radiation weighting of photon being 1 as described in an earlier section. Therefore, no explicit data of equivalent dose is presented.

As presented below, Figure 3.1 shows from the first of four sets of measurements, an exponential decline (except for an increase in the kidney dose) of measured Out-of-Field organ doses in units of cGy, resulting from a 1 fraction treatment of 200cGy delivered to the NPC treatment site, using 6MV IMRT beams from the Varian Clinac (TRILOGY). The measured doses ranged from 3.33cGy, in the brain located proximal to the NPC treatment field, to 0.04cGy in the testes located distal to the treatment field. Measurements were made in the adult male ATOM phantom with all transverse cross-sectional slices intact (Cofiguration-1).

The second set of measurements was done using TRILOGY with the ATOM phantom in configuration-2. This configuration enables the reduction of in-phantom scatter radiation to negligible levels in terms of contributing to the Out-of-Field dose. Thus resulting in the leakage radiation component of the measured Out-of-Field Organ Dose in Figure 3.2 which also shows the same exponential trend as the total dose in Figure 3.1. Measured leakage radiation values ranged from 2.49cGy in the brain located

proximal to the NPC treatment field and 0.04cGy in the testes located distal to the treatment field.

The scatter radiation component of total Out-of-Field organ dose in the TRILOGY measurement was computed as the difference between the measured total and leakage radiations under the same treatment conditions and graphically represented as shown on Figure 3.3. As a result of the computation of Out-of-Field organ dose coupled with the stochastic nature of organ dose, unphysical results were obtain in the stomach (-0.004cGy) and testes (-0.011cGy). Consequently the negative values where assumed to be zero values in the stomach and testes as seen on Figure 3.3, which represented the decreasing influence of scatter radiation in the total Out-of-Field dose at organ points distal to the treatment site.

In Figures 3.4 and 3.5, ratios of the two components of Out-of-Field dose considered in this work, relative to measured total Out-of-Field organ doses, are presented graphically. As presented, the ratio of scatter radiation dose ranged from 0-25% in Figure 3.4, also the ratio of leakage radiation dose ranged from 75% to 100% as shown in Figure 3.5

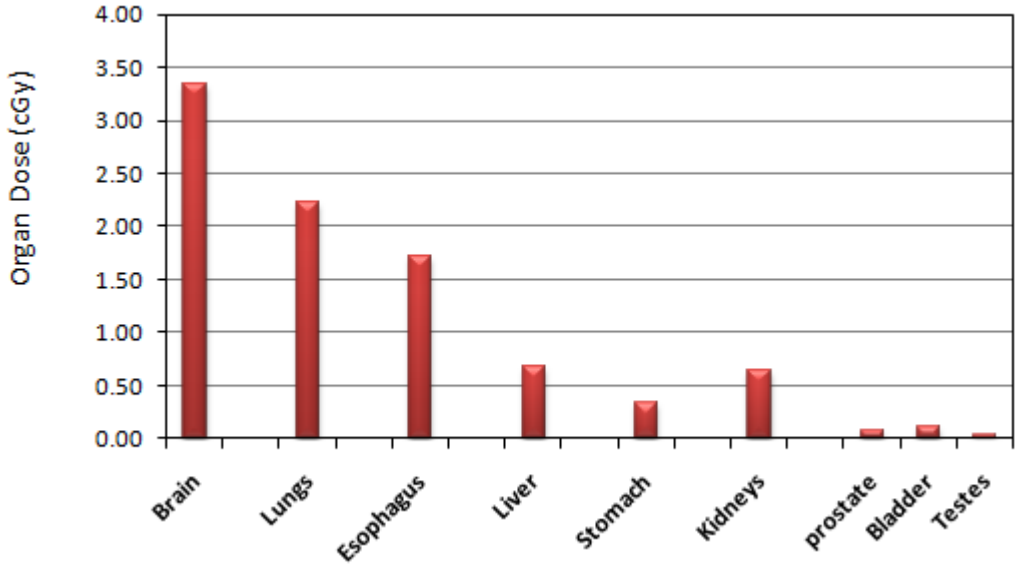

Figure 3.1 Total Out-of-Field Organ Dose Measured in-vivo, using the Adult Male ATOM Phantom and the Varian TRILOGY, in which all the transverse Slices of the phantom are in place(Configuration-1). A total of 200cGy was delivered to the tumor target in 1 fraction of IMRT of NPC.

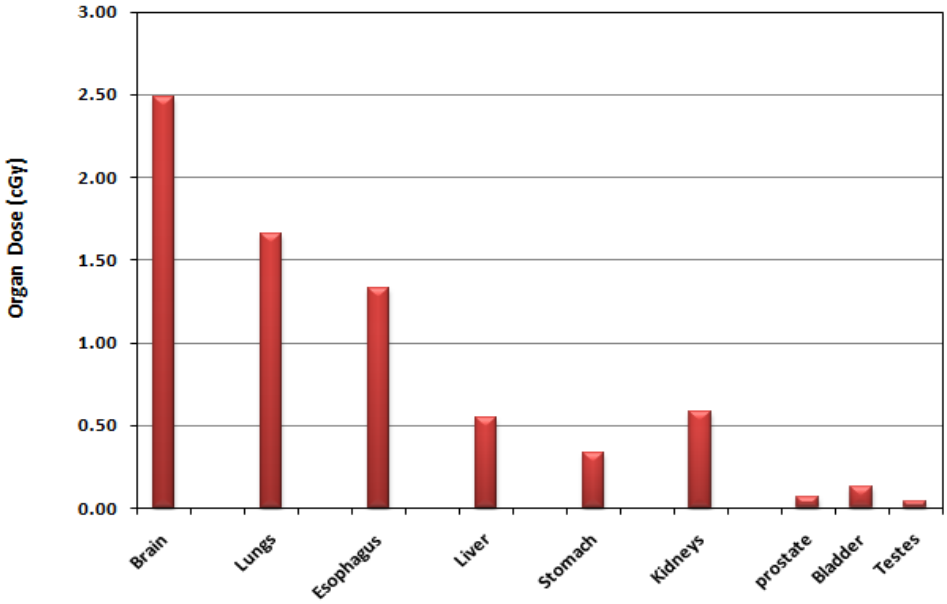

Figure 3.2 Leakage Radiation Organ Dose Component of the Total Out-of- field Radiation Dose. Measured in the Adult Male ATOM phantom with the transverse Slices in the treatment field removed from the Atom Phantom (Configuration-2) to eliminate in-patient scatter, under the same treatment conditions as Configuration-1 using TRLOGY to deliver 200cGy in 1 treatment-fraction of IMRT of NPC.

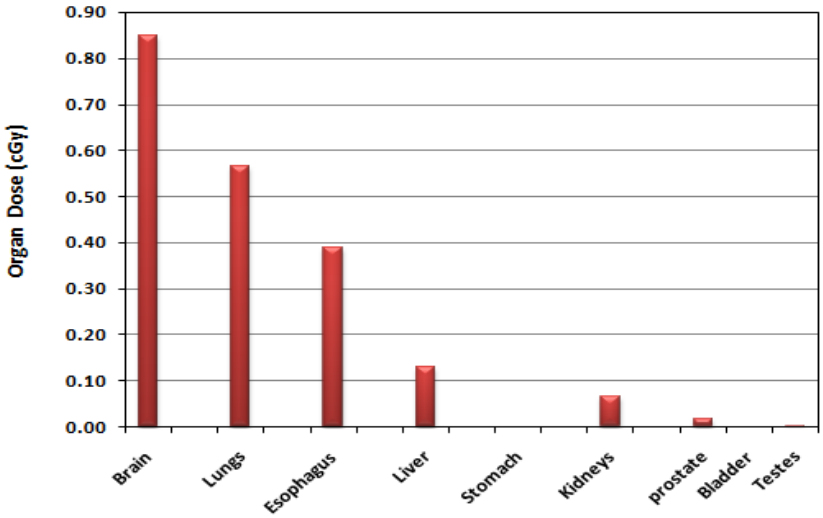

Figure 3.3 Computed Scatter Radiation Organ Dose Component of the Total Out-of-field Radiation Dose, derived as the difference between the measured (Total Out-of-Field dose and Leakage Radiation Dose Component) values in the Adult Male ATOM phantom, as a result of IMRT of NPC using TRILOGY.

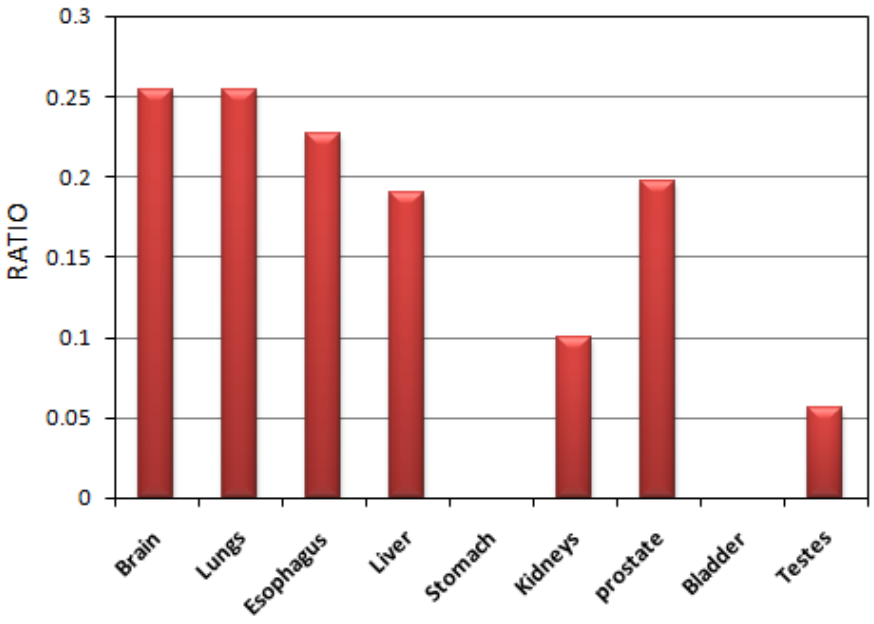

Figure 3.4 Computed Ratio of Scatter Radiation dose to Total Out-of-field Organ dose based on IMRT of NPC using TRILOGY.

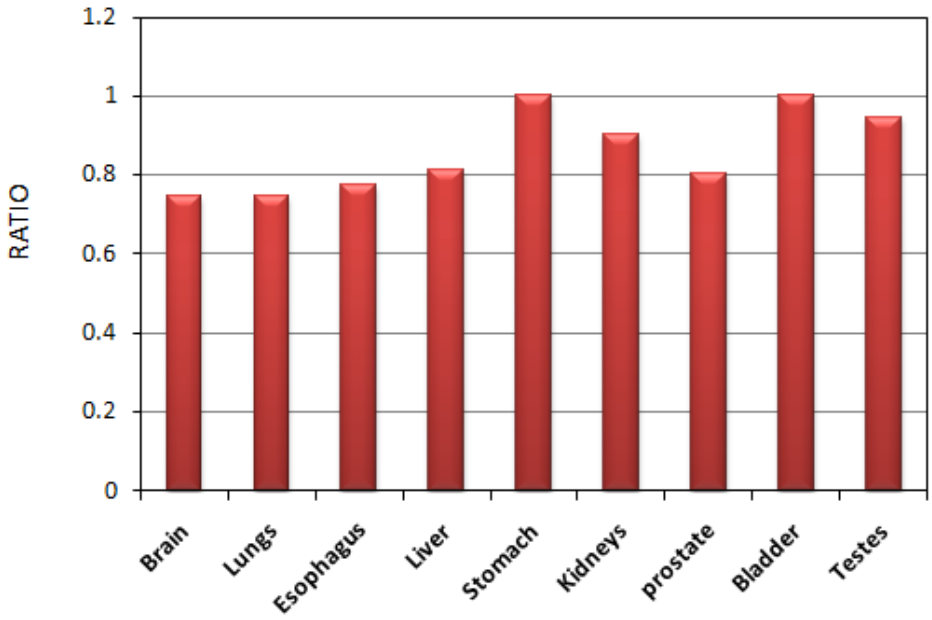

Figure 3.5 Computed Ratio of Leakage Radiation dose to Total Out-of-field Organ dose based on IMRT of NPC using TRILOGY.

3.2 Head and Neck Helical TomoTherapy Out-of-Field Organ and Equivalent Dose Results

Like the previous section, in this section a graphical presentation is given of the measurements and computations of Out-of-Field organ dose, but specific to the TomoTherapy® Hi-Art® II delivery system (TOMO). Shown in Figure 3.6 is the result of the 3rd set of measurements, reflective of the characteristic exponential decline (except for an increase in the kidney dose similar to TRILOGY, but of a smaller magnitude) of measured Out-of-Field organ doses in units of cGy, resulting from similar treatment condition highlighted in the previous section, in which a 1 fraction treatment of 200cGy delivered to the NPC treatment site, but using 6MV helical TomoTherapy beams. The measured doses ranged from 2.75cGy, in the brain located proximal to the NPC treatment field, to 0.15cGy in the prostate gland located distal to the treatment field. Measurements were also made in the adult male ATOM phantom with all transverse cross-sectional slices intact (Cofiguration-1).

The fourth and final set of measurements in this work was done using TOMO with the ATOM phantom in configuration-2 enabling the measurement of the leakage radiation component of the measured Out-of-Field Organ Dose, as shown in Figure 3.7 The measurements were done under the same treatment conditions as the previous 3 measurements delivering 7000cGy to the treatment site (NPC) using IMRT. The organs proximal to the treatment site (brains and lungs) are observed to have the highest levels of leakage doses. A slight variation in the exponential trend of Out-of-Field dose is observed in Figure 3.7 due to the locations of the organs (brains and lungs) with respect to the treatment site. The brain is located superior to the treatment site while the lungs are inferior to the treatment site, lying on the same side with all other organs studied in this work thus resulting in the characteristic exponential decline beyond the lungs. Measured leakage radiation values ranged from 0.67cGy in the brain to 0.15cGy in the prostates.

The scatter radiation component of total Out-of-Field organ dose in TOMO measurement was also computed as the difference between the measured total and leakage radiations under the same treatment conditions and graphically represented as shown on Figure 3.8. Similar to the TRILOGY computations, unphysical results were

also obtained in TOMO computations. However, the organs associated with the negative results changed in one instance from stomach in TRILOGY to the bladder in TOMO. The computed negative values were -0.27cGy (bladder) and -0.40cGy (testis). Consequently the negative values where assumed to be zero values in the bladder and testis as seen on Figure 3.8, which also is representative of the decreasing influence of scatter radiation in the total Out-of-Field dose at organ points distal to the treatment site, similar to behavior observed in the TRILOGY measurements .

Similar to TRILOGY, the ratios of the two components of Out-of-Field dose considered in this work, relative to measured total Out-of-Field organ doses, are presented graphically in Figures 3.9 and 3.10. The ratios of scatter radiation dose, ranged from 0-75% in Figure 3.9, likewise the ratio of leakage radiation dose ranged from 25% to 100% as shown in Figure 3.10, for TOMO.

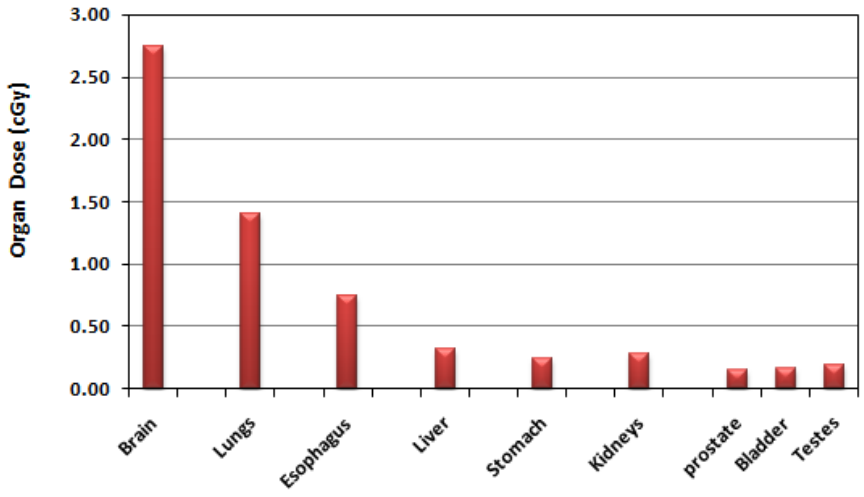

Figure 3.6 Total Out-of-Field Organ Dose Measured in-vivo, using the Adult Male ATOM Phantom and the TomoTherapy® Hi-Art® II system, in which all the transverse Slices of the phantom are in place(Configuration-1). A total of 200cGy was delivered to the tumor target in 1 fraction of IMRT of NPC.

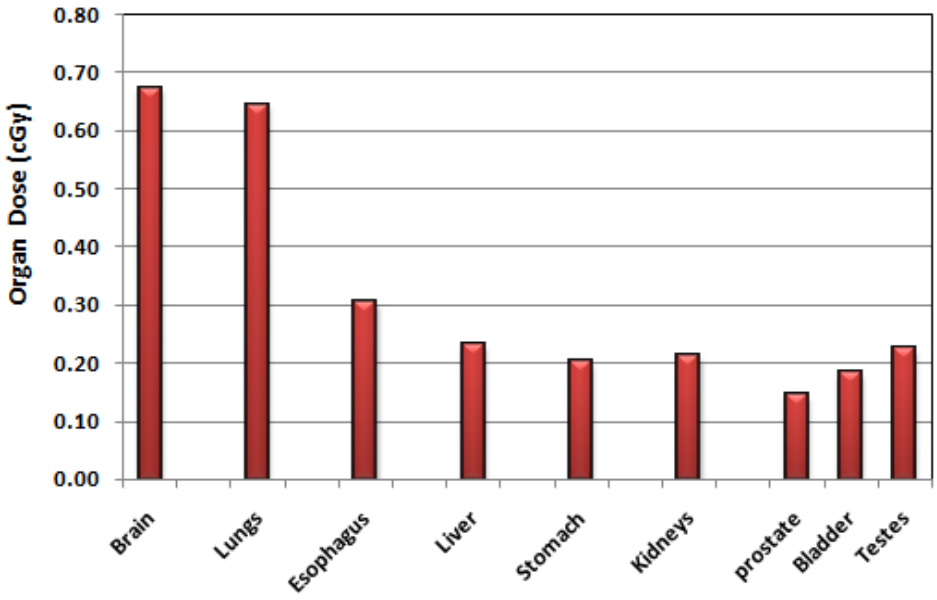

Figure 3.7 Leakage Radiation Organ Dose Component of the Total Out-of- field Radiation Dose. Measured in the Adult Male ATOM phantom with the transverse Slices in the treatment field removed from the Atom Phantom (Configuration-2) to eliminate in-patient scatter, under the same treatment conditions as Configuration-1 using TomoTherapy® Hi-Art® II system to deliver 200cGy in 1 treatment-fraction of IMRT of NPC.

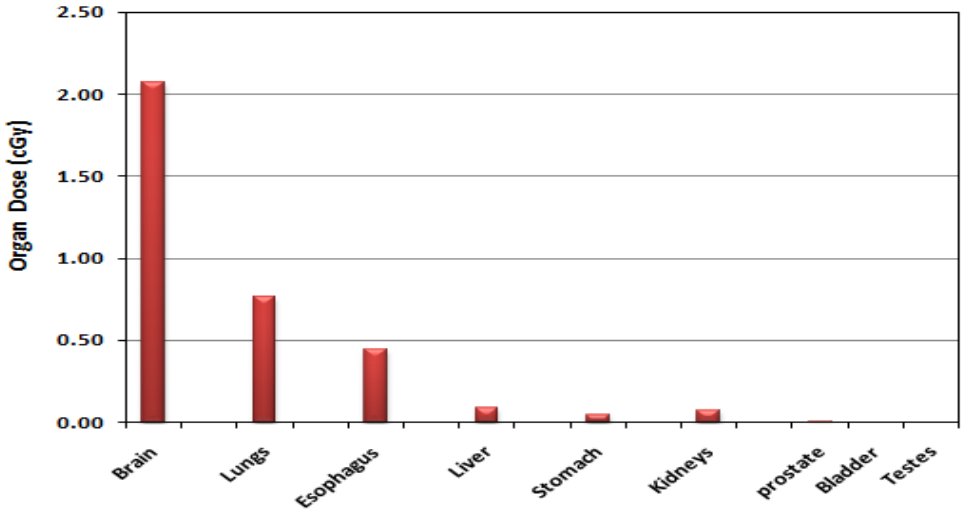

Figure 3.8 Computed Scatter Radiation Organ Dose Component of the Total Out-of-field Radiation Dose, derived as the difference between the measured (Total Out-of-Field dose and Leakage Radiation Dose Component) values in the Adult Male ATOM phantom, as a result of IMRT of NPC using TomoTherapy® Hi-Art® II system.

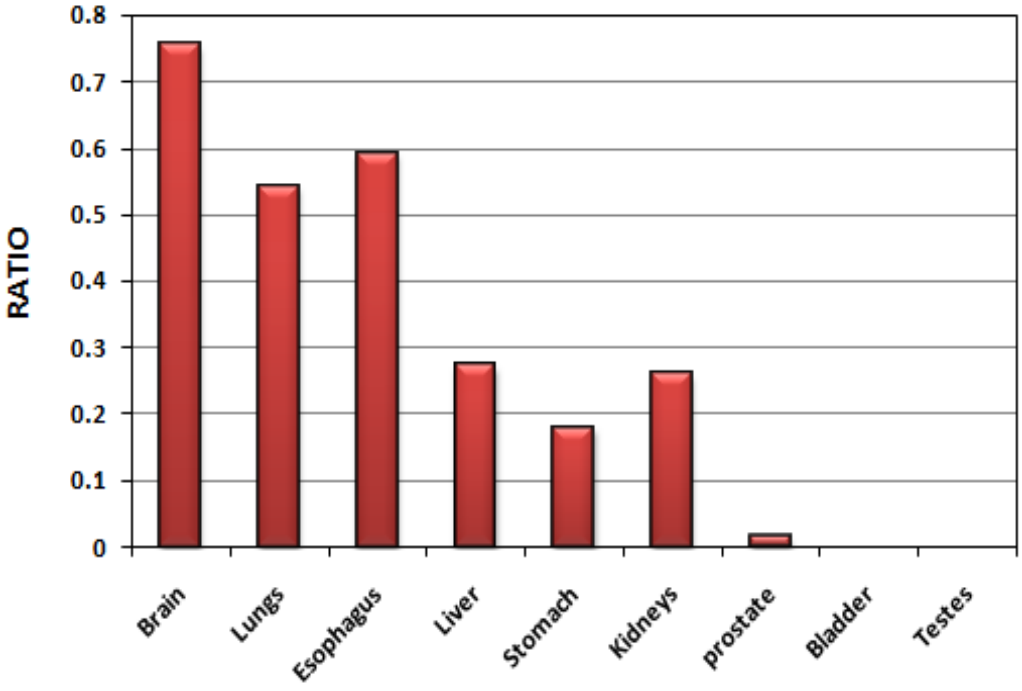

Figure 3.9 Computed Ratio of Scatter Radiation dose to Total Out-of-field Organ dose based on IMRT of NPC using TomoTherapy® Hi-Art® II system.

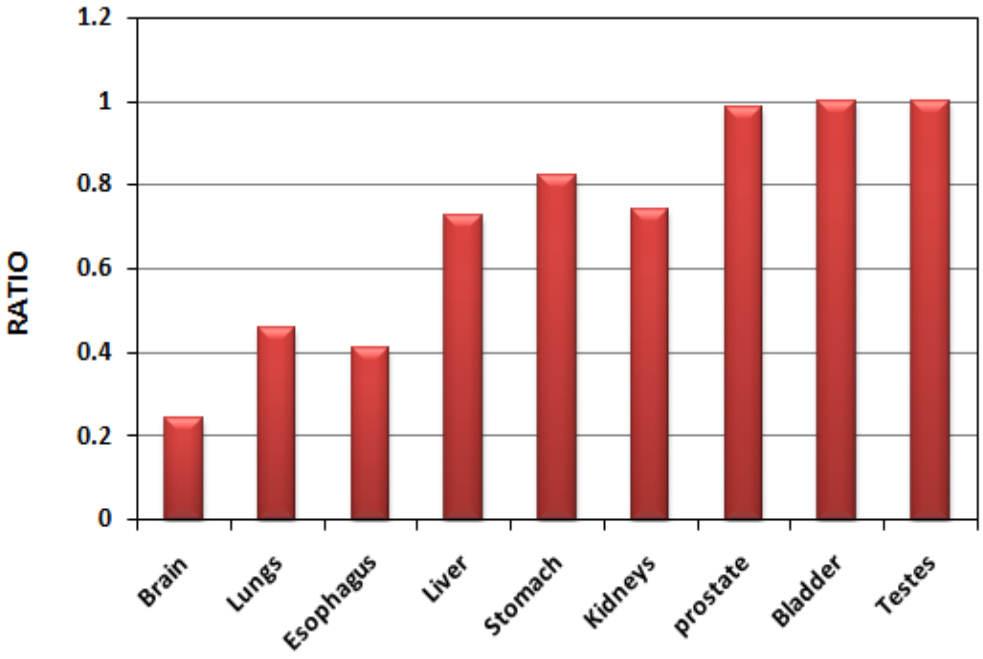

Figure 3.10 Computed Ratio of Leakage Radiation dose to Total Out-of-field Organ dose based on IMRT of NPC using TomoTherapy® Hi-Art® II system.

3.3 Analysis of Out-of-Field Dose from Varian Clinac and Helical TomoTherapy Delivery

In comparing the Out-of-field organ dose computed from the measurements, certain trends were observed. The measurement setup was based on similar treatment conditions such as: same patient, same NPC Tumor Volumes – GTV, PTV, and PTV59-PTV, Same treatment modality –IMRT, same treatment energy – 6MV, same treatment goals and same OAR constraints. Also different treatment systems (Varian TRILOGY delivery system and TomoTherapy Hi-Art II delivery systems) using different treatment plans to achieve the same treatment goal of dose escalation to tumor site and dose avoidance to OAR was also adopted. Consequently different on-board imaging modalities (MVCT and KBCBCT) using different energies for daily patient imaging before treatment was also considered in this work, thus taking note of the additional contributing of imaging-dose to organs Out-of-field, as highlighted by Murphy et al. in introducing work on AAPM TG 75 regarding radiation dose delivered via image guidance techniques during radiotherapy, where its stated "Although widely varied in modality and method, all radiographic guidance techniques have one thing in common—they can give a significant radiation dose to the patient. As with all medical uses of ionizing radiation, the general view is that this exposure should be carefully managed" (Murphy et al. 2007) and further emphasized buy Aird that "because this cumulative extra-target dose has a negative biological effect even within the context of radiotherapy, it is important that the radiation therapy community assess its cost and benefit" (Aird 2004).

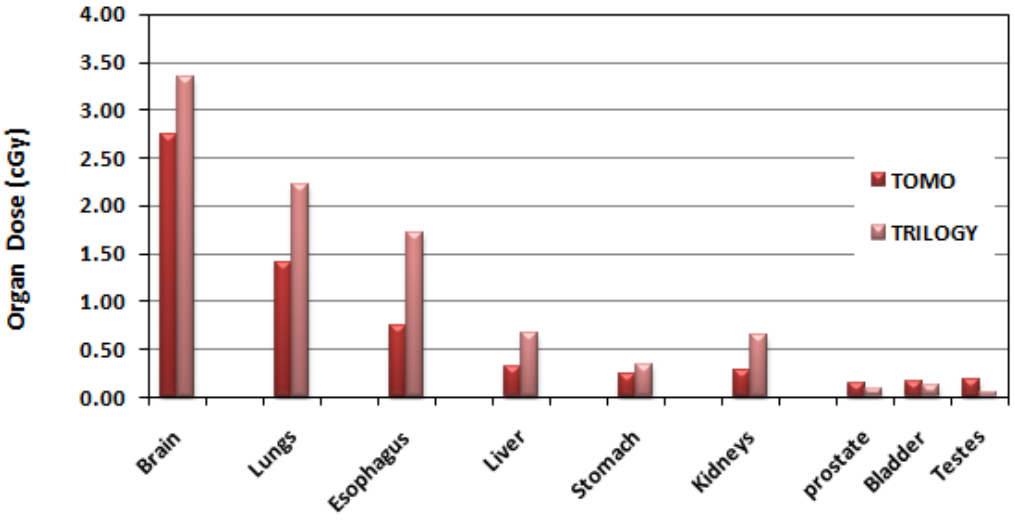

Figure 3.11 Comparison-Plots of Total Out-of-Field Organ Dose Measured in-vivo, using the Adult Male ATOM Phantom and the TomoTherapy® Hi-Art® II system and the Varian TRILOGY delivery system, in which all the transverse Slices of the phantom are in place(Configuration-1). A total of 200cGy was delivered to the tumor target in 1 fraction of IMRT of NPC.

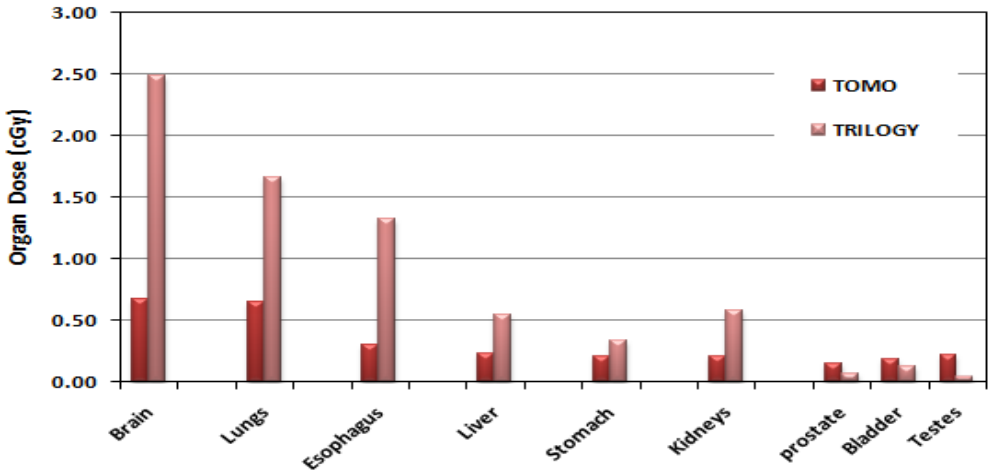

Figure 3.12 Comparison-Plots of Leakage Radiation Organ Dose Component of the Total Out-of- field Radiation Dose. Measured in the Adult Male ATOM phantom with the transverse Slices in the treatment field removed from the Atom Phantom (Configuration-2) to eliminate in-patient scatter, under the same treatment conditions as Configuration-1 using TomoTherapy® Hi-Art® II system and Varian TRILOGY delivery system, to deliver 200cGy in 1 treatment-fraction of IMRT of NPC.

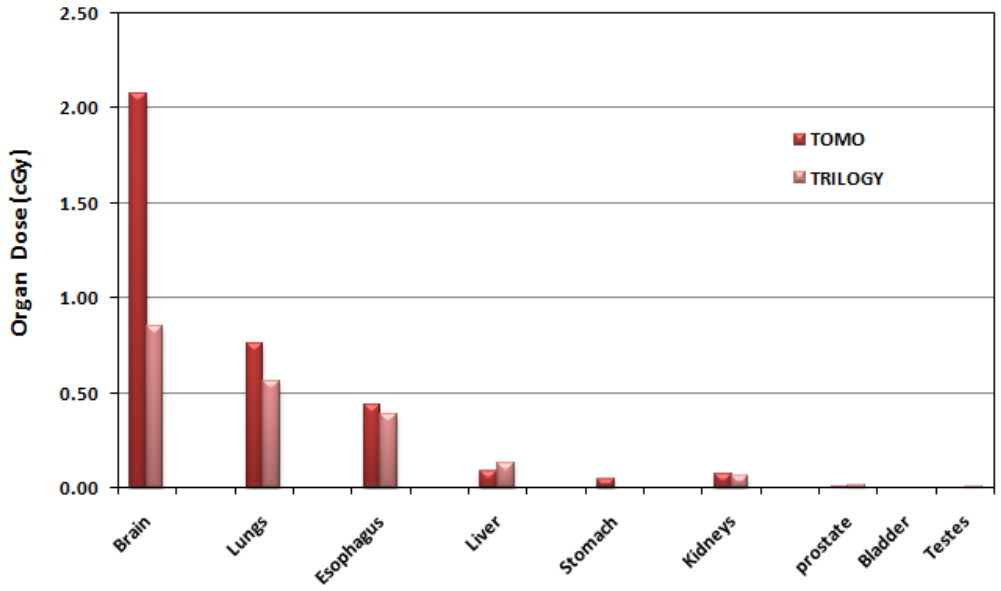

Figure 3.13 Comparison-Plots of Computed Scatter Radiation Organ Dose Component of the Total Out-of-field Radiation Dose, derived as the difference between the measured (Total Out-of-Field dose and Leakage Radiation Dose Component) values in the Adult Male ATOM phantom, as a result of IMRT of NPC using TomoTherapy® Hi-Art® II system and Varian TRILOGY delivery system.

Total Out-of-field dose trended exponentially in both TOMO and TRILOGY Figure 3.11 like the data in the literature (Meeks et al. 2002, Ramsey et al. 2006, Sharma et al. 2006), however, the methods adopted in this work enabled the direct measurement of the leakage-radiation component due to IMRT of NPC using both TOMO and TRILOGY and the derivation of scatter-radiation component of the total Out-of-Field organ dose. Consequently, it is observed that the ratio of scatter radiation to total dose, trended in a different manners between both treatment systems as shown in Figure 3.14, the actual measured leakage radiation ratio also behaved differently at distances proximal to the treatment field as shown in Figure 3.15. It is observed that the scatter radiation component from TRILOGY contributes the smaller portion of the total dose, ranging between 25-0% while the leakage radiation component contributes the larger portion of the total dose, ranging between 75-100% of the total Out-of-field dose to organs spread across the full length of the Adult male ATOM phantom from the brain along the superior-inferior (z-axis) direction from the isocenter of the treatment field to the testes.

Both ratios of scatter and leakage radiation changed slowly along the Z-axis direction from the Brain to the testes in the case of TRILOGY.

On the contrary, It is observed that the scatter radiation component from TOMO contributes an almost symmetrical portion of the total dose, ranging from 75 - 0% while the leakage radiation component contributes symmetrically to the total dose, ranging between 25-100% of the total Out-of-field dose, both scatter and leakage radiation contribution ratios seem to be evenly decreasing and increasing respectively at the same time. The difference in the behavior of the scatter and leakage components could be attributed to the mode of IMRT delivery of both modalities. TOMO has helical delivery thus a more symmetrical deposition while the TRILOGY delivery is dependent on the beam angles determined in the treatment plan, in this work most of the delivery was posterior to anterior (PA).

Also, in comparing the total Out-of-field organ dose in terms of delivery systems, TRILOGY was observed to deliver a higher dose to the organs proximal to the treatment field: brain, lungs, esophagus, liver, stomach and kidney; while TOMO delivered more dose to organs distal to the treatment field - prostate, bladder and testes as seen earlier in Figure 3.11. A table showing the percentages of Out-of-field organ dose per treatment fraction for each organ studied is presented in Table 3.3.1, where values range from 0.02 – 1.67% in the testes and brain respectively for the TRILOGY and 0.07 – 1.37% in TOMO.

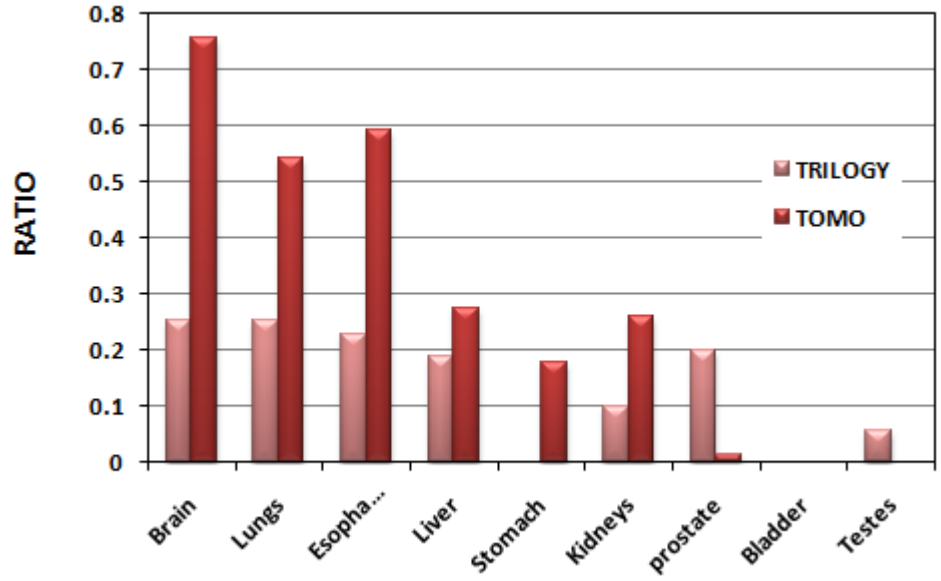

Figure 3.14 Comparison-Plots of Computed Ratio of Scatter Radiation dose to Total Out-of-field Organ dose based on IMRT of NPC using Varian TRILOGY delivery system and TomoTherapy® Hi-Art® II system.

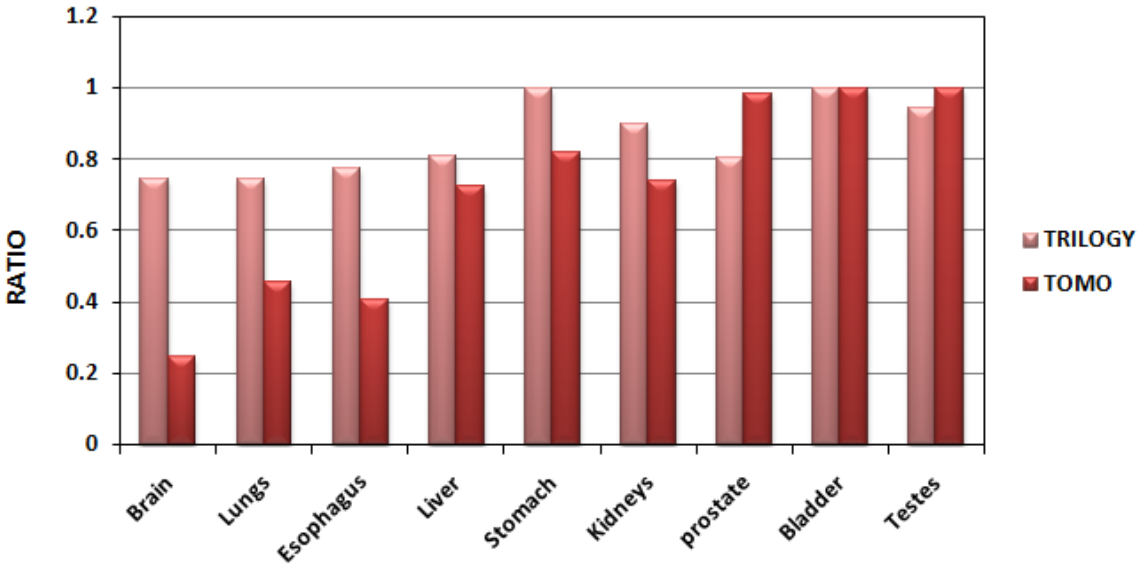

Figure 3.15 Comparison-Plots of Computed Ratio of Leakage Radiation dose to Total Out-of-field Organ dose based on IMRT of NPC using Varian TRILOGY delivery system and TomoTherapy® Hi-Art® II system.

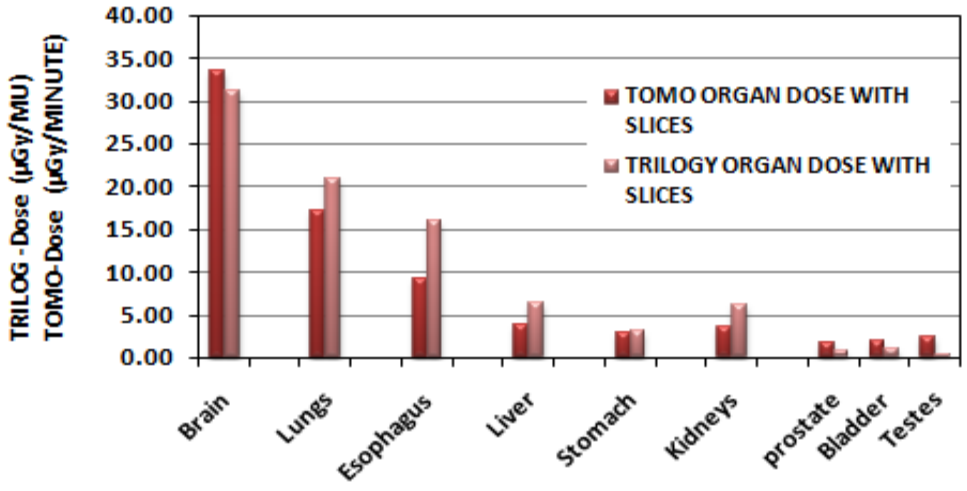

Figure 3.16 Comparison-Plots of Total Out-of-Field Organ Dose Measured in-vivo, using the Adult Male ATOM Phantom, with values normalize to treatment time in TomoTherapy® Hi-Art® II system and values normalized to MU for Varian TRILOGY delivery system, in which all the transverse Slices of the phantom are in place(Configuration-1). A total of 200cGy was delivered to the tumor target in 1 fraction of IMRT of NPC.

Table 3.3.1 Percentages of Out-of-field organ dose per treatment fraction in which 200cG was delivered to the treatment site.

ORGANS	**TRILOGY Organ Dose Percentage per fraction of 200cGy**	**TOMIO Organ Dose Percentage per fraction of 200cGy**
Brain	1.67%	1.37%
Lungs	1.11%	0.70%
Esophagus	0.86%	0.37%
Liver	0.34%	0.16%
Stomach	0.17%	0.12%
Kidneys	0.32%	0.14%
Prostate	0.04%	0.07%
Bladder	0.06%	0.08%
Testes	0.02%	0.09%

Finally, in comparing the delivery systems based on beam on time and beam output, it is noted that reduction of MU was significant in reducing Out-of-field organ dose in IMRT plans for linac systems like TRILOGY, while the reduction of treatment-time was significant in the same sense for TOMO. Thus, a comparison is graphed on Fig 3. 16 to showing dose normalized to MU and treatment-time. It's observed that the trend and values of dose deposited by both systems based on MU and treatment-time are in good agreement with the trend and values based on a similar comparison of total dose deposited. These point to a possible equivalence or relationship between treatment-time in helical TOMO delivery and MU in TRILOGY linac delivery of external beam radiation.

3.4 Comparative Analysis of Results from this Study and Data from Literature

In the literature it is observed that there is an exponential decrease in the out-of-field organ doses which correlates with previous work (Meeks et al. 2002, Ramsey et al. 2006, Sharma et al. 2006). However the dearth of out of field dose data specific to IMRT of NPC due to the complexity of NPC treatment is observed. The complexity of NPC seems to skew the focus of critical organ sparing to OAR in field due to radiation therapy. The varied possibility of generating different TP's, based on planner-experience, to treat the same kind of NPC also makes it difficult to accurately compare data from this work to literature. Thus the motivation to generate in this work, similar TP's for the same NPC to be delivered to an anthropomorphic phantom by two systems for the basis of comparison. Hopefully this will introduce a new and balanced approach to solve the important problem of choosing the optimal delivery system to adopt in complex cases of cancer treatment; consequently making a difference in improving treatment outcome and quality of life for patients (especially younger patients that have a better chance of living longer). This work should encourage the gathering of comparative data in a similar manner to eventually be used in developing a computational model that can assist clinicians choose the best delivery system for complex cases as they arise. Also it is observed that a facility could have various viable

options to choose from in the face of a variety of complex cancer problems, having complex biological and geometrical variations. Thus choosing the right delivery system could make a difference in reducing total non-target dose to as low as reasonably achievable levels as well as make a difference in terms of quality of life for the patient after treatment.

The methods adopted in this work enabled the direct measurement of the leakage-radiation component due to IMRT of NPC using both TOMO and TRILOGY and the derivation of scatter-radiation component of the total out-of-field organ dose while imbedding the dose due to the on-board imaging modalities of both systems. (Murphy et al. 2007) pointed to the fact that scatter dose had been reported to decrease exponentially based on other works in the literature stating "In a clinical case study of one example prostate IMRT treatment, Cigna et al. (2004) measured the total scattered dose from both internal and external 6 MV Varian Clinac 6/100 sources using ten pen dosimeters arranged at various points on the surface of the patient's body. Again, the geometrical distribution of scattered dose fell off steeply with distance from the target"(Murphy et al. 2007) in which a dose of 70.2Gy dose was delivered to the prostate tumor target. However, this theses work shows that the ratio of the scatter radiation component of total dose does not correspond to the geometrical exponential decline of scatter dose. This deviation is shown by the slow fall of in the ratio of scatter radiation dose to total out-of-field organ dose for the TRILOGY delivery system as compared to the TOMO system which showed the characteristic exponential decline in the ratio of scatter to total dose Figure 3.13. These points to the need for further investigation of the varied behavior of scatter and leakage radiation dose contribution to Organs outside the treatment field.

Also in regards to estimating concomitant imaging dose, associated challenges range from the complex relationship between Out-of-field dose contribution from the radiation therapy modality used and its associated treatment conditions (position of treatment site, patient shape and size and geometry of treatment fields) which is patient specific in most cases. However, the importance of assessing the concomitant imaging dose contribution to Out-of-Field organ dose during radiation therapy cannot be overemphasized, given that imaging dose contributions could be widespread ranging

from skin dose to organ outside the treatment field receiving radiation therapy. Consequently it is suggested that the methods adopted in this work, makes it possible to asses concomitant imaging dose by taking measurements without the treatment slices in place – eliminating scatter dose, and then taking two similar measurements with the same treatment conditions, one with the imaging modality in place measuring imaging-dose and leakage radiation and the next without the imaging modality using detectors sensitive to the radiation level of imaging dose. Thus the difference of the latter two measurements (leakage minus (leakage + Imaging-dose)) gives an estimate of imaging dose for the treatment conditions being tested.

4. Conclusions

The need to improve current treatment planning by factoring the out-of-field dose to healthy organs and consequently improving treatment outcomes and quality of life of patients as well as reducing the risk of secondary cancer due to external beam radiation treatment is the underlying motivation of this work. Currently there are no established computational tools that can effectively estimate and predict such dose and risk to organs outside the treatment field. Also there is limited specific-data on organ dose outside the treatment volume regarding different modalities adopted for radiation therapy. The analysis and results in this work show a similar trend in the total out-of-field organ dose. However in this study, there is a marked difference in the specific behavior of the scatter-components of out-of-field organ dose for TRILOGY showing a slow and not-so-steep decline. Thus the limited body of work already done in regards to out-of-field dose measurements leaves room for more in depth studies involving comparisons of new and emerging modalities for radiation therapy in the clinic. However, the challenge to implement these out-of-field data in treatment planning remains and is beyond the scope of this study.

One of the goals in on-going research at many centers is the development of improved methods as well as a computational tool to enable better treatment delivery to patients through the proper prediction of organ dose outside field of treatment to complement in-field dose estimates and enhance a more accurate understanding of total organ dose due to radiation therapy, proper estimation of secondary cancer risk and finally the factorization of these findings to the final treatment plan for patients. This goal will be less challenging when we have acquired and understood a large data base of actual measurement of a variety or radiation therapy modalities which can provide the raw data for the development of an effective computational tool. More work needs to be done in the future in regards to accumulation of data as the use of radiation expands, in order to have adequate data base to enable the development of theoretical computational tools based on practical experimental data.

REFERENCES

Aird EGA. Second cancer risk, concomitant exposures and IMRER(2000). The British Journal of Radiology 77: 983-985; 2004.

Attic FH. Introduction to radiological physics and radiation dosimetry. Weinheim: WILEY-VCH Verlag GmbH & Co. KGaA; 2004.

Bednarz BP. Detailed Varian clinac accelerator modeling for calculating intermediate and low-level non-target organ doses from radiation treatments. PhD Theses. Rensselaer Polytechnic Institute. Troy, NY: 2008

Bortfeld T. IMRT: A review and preview. Phys Med Biol 51: 363-379; 2006.

Brahme A. Optimization of stationary and moving beam radiation therapy techniques. Radiotherapy and Oncology 12: 129-140; 1988.

Brahme A, Roos JE, Lax I. Solution of an integral equation encountered in rotation therapy. Phys Med Biol 27: No.10; 1221-1229; 1982.

Cigna AA, Nassisi D, Masenga D, Raffo R, Rotta P. Dose due to scattered radiation in external radiotherapy: A prostate cancer case history. Radiation Protection Dosimetry 108: No. 1; 27-32; 2004.

CIRS Tissue Simulation Technology. Dosimetry Verification Phantoms. Available at: http://www.cirsinc.com/pdfs/700cp.pdf . Accessed 14 January 2009.

Diallo I, Lamon A, Shamsaldin A, Grimaud E, de Vathaire F, Chavaudra J . Estimation of the radiation dose delivered to any point outside the target volume per patient treated with external beam radiotherapy. Radiotherapy and Oncology 38: 269–271; 1996.

Dong L, Mohan R. Intensity-modulated radiation therapy physics and quality assurance. In: Chao Clifford KS, Apisarnthanarax S, Ozyigit G, eds. Practical essentials of intensity modulated radiation therapy, 2nd ed. Philadelphia, PA: Lippincott Williams & Wilkins; 1-19; 2005.

EduCase: IMRT Contouring Tool. Available at: http://www.educase.com/. Accessed 14 January 2009.

Fraass BA, Van De Geijn J. Peripheral dose from megavolt beams. Med. Phys 10: 809–818; 1983.

Francois P, Beurtheret C, Dutreix A. Calculation of the dose delivered to organs outside the radiation beams. Med Phys 15: 879–883; 1988.

Geara FB, Sanguineti G, Tucker SL, Gareden AS, Ang KK, Morrison WH, Peters LJ. Carcinoma of the nasopharynx treated by radiotherapy alone: determinants of distant metastasis and survival. Radiotherapy and Oncology 43: 53-61; 1997.

Greene FL, Sobin LH. The staging of cancer: A retrospective and prospective appraisal. CA Cancer J Clin 58: 180-190; 2008.

Howell RM, Hertel NE, Wang Z, Hutchinson J. Calculation of effective dose from measurements of secondary neutron spectra and scattered photon dose from dynamic MLC IMRT for 6 MV 15MV and 18MV beam energies.
Med Phys 33: No. 2; 360-368; 2006

Hunt MA, Zelefsky MJ, Wolden S, Chui C, Losasso T, Rosenzweig K, Chong L, Spirou SV, Fromme L, Lumley M, Amols HA, Ling CC, Leibel SA. Treatment planning and delivery of intensity-modulated radiation therapy for primary nasopharynx cancer. Int J Radiat Oncol Biol Phys 49: No.3; 623-632; 2001.

International Commission on Radiological Protection (ICRP) Publication 92. Valentine J ed. Relative Biological Effectiveness (RBE), QualityFactor (Q), and Radiation Weighting Factor (w_R): Elsevier Ltd; 2003

International Commission on Radiation Units (ICRU) Report 50. Prescribing Recording and Reporting Photon Beam Therapy: Bethesda, MD; 2003.

Intensity Modulated Radiation Therapy Collaborative Working Group (IMRT-CWG). Intensity modulated radiation therapy: current status and issues of interest. Int J Radiat Oncol Biol Phys 51: 880-914; 2001.

Kase KR, Svensson GK, Wolbarst AB and MarksMA. Measurement of dose from secondary radiation outside a treatment field. Int J Radiat Oncol Biol Phys 9**:**1173–83; 1983.

Khan FM. The physics of radiation therapy, 3rd ed. Philadelphia, PA: Lippincott Williams & Wilkins; 2003.

Knoll GF. Radiation detection and measurement, 3rd ed. Hoboken, NJ: John Wiley & Sons; 2000.

Kry SF, Price M, Followill D, Mourada F, Salehpour M. The use of LiF (TLD-100) as an out-of-field dosimeter. J of Applied Clinical Med Phys 8: No. 4:169-175; 2007a.

Kry SF, Titt U, Followill D, Pönisch F, Vassiliev ON, White RA, Stovall M, Salehpour M. A monte carlo model for out-of-field dose calculation from high energy photon therapy. Med Phys 34: No.9; 3489-3500; 2007b.

Kry SF, Titt U, Pönisch F, Followill D, Vassiliev ON, White RA, Mohan R, Salehpour M. A monte carlo model for out-of-field dose calculation from high energy photon therapy. Med Phys 33: No.11; 4405-4413; 2006.

Lee NY, Chao Clifford KS. Nasopharynx. In: Chao Clifford KS, Apisarnthanarax S, Ozyigit G, eds. Practical essentials of intensity modulated radiation therapy, 2nd ed. Philadelphia, PA: Lippincott Williams & Wilkins; 2005: 20-29.

McParland BJ, Fair HI. A method of calculating peripheral dose distributions of photon beams below 10 MV. Med Phys 19: 283–93; 1992.

Meeks SL, Paulino AC, Pennington EC, Simon JH, Skwarchuk MW, Buatti JM. In vivo determination of extra-target doses received from serial TomoTherapy. Radiotherapy and Oncology 63: 217-222; 2002.

Murphy MJ, Balter J, Balter S, BenComo JA Jr, Das IJ, Jiang SB, Ma CM, Olivera GH, Rodebaugh RF, Ruchala KJ, Shirato H, Yin FF. The management of imaging dose during image-guided radiotherapy AAPM TG 75. Med Phys 34: No. 10; 4041 – 4063; 2007.

Mutic S, Low DA. Whole-Body dose from Tomotherapy delivery. Int J Rad Oncol Biol Phys 42: No. 1; 229-232; 1998.

Qin D, Hu Y, Yan J, Xu G, Cai W, Wu X, Cao D, Gu X. Analysis of 1379 patients with nasopharyngeal carcinoma treated by radiation. Cancer 61: 1117-1124; 1988.

Radiation Therapy Oncology Group (RTOG) 0225 A Phase II Study of Intensity Modulated Radiation Therapy (IMRT) +/- Chemotherapy for Nasopharyngeal Cancer. Available at: http://www.rtog.org/members/protocols/0225/0225.pdf Accessed 14 January 2009.

Ramsey CR, Seibert R, Mahan SL, Desai Dharmin, Chase D. Out-of-field Dosimetry Measurements for a Helical Tomotherapy system. Journal of applied clinical med phys 7: No 3; 2006.

Roentgen Wilhelm. On a new kind of rays. Read before the Würzburg physical and medical society, 1895. Available at http://web.lemoyne.edu/~giunta/roentgen.html . Accessed 14 February 2009

Sharma SD, Upreti RR. Deshpande DD. Use of peripheral dose data from uniform dynamic multileaf collimation fields to estimate out-of-field organ dose in patients treated employing sliding window intensity-modulated radiotherapy. Phys Med Biol 51: 29870-1995; 2006.

Sharma SD, Upreti RR, Laskar S, Tambe CM, Deshpande DD, Shrivastava SK, Din shaw KA. Estimation of risk of radiation-induced carcinogenesis in adolescents with nasopharyngeal cancer treated using sliding window IMRT. Radiotherapy and Oncology 86: 177-181; 2008.

Sherazi S, Kase KR. Measurements of dose from secondary radiation outside a treatment field: effects of wedges and blocks. Int J Radiat Oncol Biol 11: 2171–6; 1985.

Stevens G, Downes S, Ralston A. Thyroid dose in children undergoing prophylactic cranial irradiation. Int J Radiat Oncol Biol Phys 42: 385-390; 1998.

Stovall M, Smith SA, Rosenstein M. Tissue doses from radiotherapy of cancer of the uterine cervix. Med Phys 16: 726-733; 1989.

Stovall M, Blackwell CR, Cundiff J, Novack DH, Palta JR, Wagner EW, Shalek RJ. Fetal dose from radiotherapy with photon beam: Report of AAPM radiation therapy task group No, 36. Med Phys 22: No. 1; 63 – 82; 2005.

Trott KR. Cane we reduce the incidence of second primary malignancies occurring after radiotherapy? Radiotherapy and Oncology 91: 1-3; 2009.

Van Der Giessen PH, Bierhuizen WJ. Comparison of measured and calculated peripheral doses in patients undergoing radiation therapy. Radiotherapy and Oncology 42: 265-270; 1996

Vanhavere F, Huyskens D, Struelens L. Peripheral neutron and gamma doses in radiotherapy with an 18MV linear accelerator. Radiation Protection Dosimetry 110: No. 1-4; 607-612; 2004.

Webb S. The physical basis of IMRT and inverse planning. The British Journal of Radiology 76: 678-689; 2003a.

Webb S. Historical perspective on IMRT. AAPM Summer school : 2003b. Available at http://www.aapm.org/meetings/03SS/Presentations/Webb.pdf. Accessed 14 February 2009.

Widesott L, Pierelli A, Fiorino C, Dell'Oca I, Broggi S, Cattaneo GM, Di Muzio N, Fazio F, and Calandrino R, Schwarz M. Intensity-modulated proton therapy versus helical TomoTherapy in nasopharynx cancer: planning comparison and NTCP evaluation. Int J Radiat Oncol Biol Phys 72: No.2; 589-596; 2008.

Wolden SL, Chen WC, Pfister DG, Kraus DH, Berry SL, Zelefsky MJ. Intensity- mod ulated radiation therapy (IMRT) for nasopharynx cancer: Update of the memorial slaon-kettering experience. Int J Rad Onc Biol Phys 64: No.1; 57-62; 2006.

Wroe A, Clasie B, Kooy H, Flanz J, Schulte R, Rosenfeld A. Out-of-field dose equiva lents delivered by passively scattered therapeutic proton beams for clinically relevant field configurations. Int J Radiat Oncol Biol Phys 73: No.1; 306-313; 2009.

Xia P. Optimization of intensity-modulated radiation therapy treatment planning. In: Chao Clifford KS, Apisarnthanarax S, Ozyigit G, eds. Practical essentials of intensity modulated radiation therapy, 2nd ed. Philadelphia, PA: Lippincott Williams & Wilkins; 2005: 135-152.

Xu XG, Bednarz B, Paganetti. A review of dosimetry studies on external-beam radiation treatment with respect to second cancer induction. Phys Med Biol 53: 193-241; 2008.